Grazing X-Ray Analysis

Abbas Alshehabi

Kyoto University

February, 2012

Preface

Grazing incidence and grazing scattering X-ray analysis techniques have been greatly used in characterizing chemical and physical propoerties of materials recently. When an X-ray beam penetrates a material at below the critical angle, the X-ray beam is totally reflected providing less inelastic scattering, enhanced sensitivity and more detection limit. This phenomenon made the foundation for several techniques like grazing emission X-ray analysis, X-ray reflectivity (XRR), and total reflection X-ray photoelectron spectroscopy (TRXPS).

The purpose of this thesis is to present new applications of grazing X-ray analysis techniques. It starts with a review of grazing emission X-ray analysis. In this method only X-ray emitted from small angles is detected, if the sample is irradiated at normal incidence or can be be double sensitive if irradiated at grazing incidence (Chapter 1). This part includes grazing exit X-ray fluorescence analysis (GE-XRF), grazing exit electron probe microanalysis (GE-EPMA), reflection high energy diffraction – total reflection angle X-ray spectroscopy (RHEED-TRAX), and X-ray refracted fluorescence (RXF).

Chapter 2 provides a novel technique of inclusion and impurity sample analysis by grazing-exit SEM-EDX. It provides a practical way to perfrom grazing exit analysis for inclusion and impurity by SEM-EDX with more sensitivity.

With the increase trend of portable and laboratory based instruments; Chapter 3 is devoted for a portable X-ray reflectometer (XRR) utilizing a low power (1.5 W) continuum X-ray tube for thickness measurement in nanometers. The purpose of this apparatus is to measure thicknesses of multilayers within an X-ray beam energy range of 1-9.5 keV in industrial and research environments in a reasonably short time.

In Chapter 4 and Chapter 5 total reflection X-ray photoelectron spectroscopy (TRXPS) has been used for a new application in hard disk top layer analysis. The effect of rinsing on the top layer is discussed in view of total reflection X-ray photoelectron spectroscopy (TRXPS) in Chapter 5.

Chapter 6 in the thesis is discussing intrinsic and extrinsic contributions to a plasmon peak. The extrinsic and intrinsic contributions were experimentally distinguishable for the plasmon peaks by the line width comparison. Chapter 7 is about angle resolved X-ray photoelectron spectroscopy associated plasmons. The relation between the surface and bulk plasmons at different exit and incidence angles has been discussed. It provides an insight about surface and bulk plasmons at total reflection and non-total reflection conditions.

February, 16th 2010.

Acknowledgment

This thesis would not have been possible without the support, help and supervision of Prof. Jun Kawai throughout my research. I would like to acknowledge Prof. Yasuharu Shirai and Prof. Haruyuki Inui, Kyoto University, for the critical review of this thesis and valuable comments.

The results within this thesis were obtained mainly during my stay in Japan as a research student under the Japanese Ministry of Education, Science, Sport and Culture support and I wish to thank the MEXT and Faculty Engineering at Kyoto University for offering me this opportunity.

I would like also to thank Dr. H. Takenaka (NTT-AT) for providing the sample for the X-ray reflectometer (XRR) measurement. Thanks are also due to Prof. Tsuyoshi Nakajima, Aichi Institute of Technology, for the comments advice about C-F bonds and Prof. Ernst G. Bauer, Arizona State University, for the useful comments about hard disk top layer analysis by total reflection X-ray photoelectron spectroscopy (TRXPS).

I wish to express individual thanks to my colleague and friend N. Sasaki for the help, discussion and encouragement he always offered throughout my research and during the preparation of this thesis.

Thanks are due to my family and friends who supported me.

Publications list

Publications related to the present thesis:

- A. Alshehabi and J. Kawai, Localised inclusion analysis of a 45o inclined small-sample holder by grazing-exit SEM-EDX, *Adv. X-Ray. Chem. Anal., Japan* **42**, 2011, 363.

- A. Alshehabi, S. Kunimura and J. Kawai, Multilayer Nano-Thickness Measurement by a Portable Low-Power Bremsstrahlung X-ray Reflectometer, *Anal. Methods*, 2010, **2**, 1555.

- A. Alshehabi, N. Sasaki and J. Kawai, Hard Disk Top- Layer Lubricant Chemical State Analysis by Total Reflection X-ray Photoelectron Spectroscopy (TRXPS), *Adv. X-Ray. Chem. Anal., Japan* **43**, 2012, in press.

- A. Alshehabi, N. Sasaki and J. Kawai, Reproducibility of Hard Disk Fluorocarbon Layer Chemical State Analysis by Total Reflection X-ray Photoelectron Spectroscopy (TRXPS), submitted.

Conferences

- **19th June, 2011:** *New techniques in grazing X-ray analysis*, Joint Symposium on Materials Science and Engineering 2011-Singapore.
- **22nd May, 2011:** *Localised inclusion analysis of a 45° inclined small-sample-holder by grazing-exit SEM-EDX*, 5th Meeting of the International Union of Microbeam Analysis Societies'2011'-'IUMAS5' Seoul (South Korea).
- **22nd May, 2011:** *Hard Disk Fluorocarbon Layer Chemical State Analysis by Total Reflection X-ray Photoelectron Spectroscopy (TRXPS)*, 9th International Symposium on Atomic Level Characterizations for New Materials and Devices ALC'11-Seoul (South Korea).
- **16th December, 2009:** *Multilayer Nano-Characterization by a Portable Bremsstrahlung X-ray Reflectometer*, 7th International Symposium on Atomic Level Characterizations for New Materials and Devices ALC'09-Hawai (USA).
- **16th December, 2009:** *Microsoft Access Database Application in Multilayer X-ray Reflectometry*, 7th International Symposium on Atomic Level Characterizations for New Materials and Devices ALC'09-Hawai (USA).

- **16th May, 2008:** *Portable x-ray reflectometer applications in multilayer and surface analysis*, The 66th Conference of the Japan Society of Analytical Chemistry, Nagoya.
- **27th November, 2007:** *Multilayer Nano-characterization by a portable X-ray reflectometer*, Japan 51st Congress of Materials Science, Kyoto.

Awards

1. "5th Meeting of the International Union of Microbeam Analysis Societies'2011'-Seoul (South Korea) 'IUMAS5'" Student Award for "***Localized Inclusion Analysis of a 45° Inclined Small-sample-holder by Grazing-exit SEM-EDX***". **(Ch.2)**

2. "7th International Symposium on Atomic Level Characterizations for New Materials and Devices '2009'ALC09'-Hawai (USA) "Student Award for "***Multilayer Nano Characterization by a Portable Bremsstrahlung X-ray Reflectometer***". **(Ch.3)**

To my parents, I dedicate this thesis.

Contents

Introducion ……………………………………………………………………1

Chapter1: Grazing Emission X-ray Analysis : A review**…………………………1**

1.1 Introduction **…………………………………………………………...2**

1.2 Principles **……………………………………………………………...4**

1.3 Reflection high energy diffraction (RHEED)**…………………………………9**

1.4 Comparison between EDXRF and WDXRF Techniques in GEXRF**………..18**

1.4.1 Resolution**………………………………..…………..............18**

1.4.2 Simultaneity **……………………………………………………...19**

1.4.3 Spectral Overlaps**……………………………..........................19**

1.4.4 Background**……………………………………………………19**

1.4.5 Excitaion Efficiency**……………………….…………………...20**

1.5 RXF (X-ray refracted fluorescence) in GEXRF**……………………………..21**

1.6 Assessment of instrument**……………………………………………………22**

1.7 Concluding Remarks**…………………………………………………………24**

References**…………………………………………………………………..25**

Figures**……………………………………………………………………...31**

Chapter 2 :Localised impurity analysis of a 45° inclined sample by grazing-exit SEM-EDX ………………………………………...………..……37

Technical Note**…………………………………………………………...37**

References**…………………………………………………………………..39**

Figures**……………………………………………………………………...40**

Chapter 3 : Multilayer Nano-Thickness Measurement by a Portable Low-Power Bremsstrahlung X-ray Reflectometer…………………………………43

3.1 Introduction**…………………………………………………….……43**

3.2 Experiment……………………………………………………………………...45
3.3 Apparatus description…………………………………………………………..45
3.4 Method description……………………………………………………………..46
3.5 Results and discussion…………………………………………………………47
3.6 Conclusion……………………………………………………..……….....50
References…………………………………………………………………………..53
Figures……………………………………………………………………………55

Chapter 4: Analysis of a Hard Disk Top- Layer by Total Reflection X-ray Photoelectron Spectroscopy (TRXPS) ……………………………………..63
4.1 Introduction……………………………………………………………………..63
4.2 Experimental……………………………………………………………………64
4.3 Results and discussion…………………………………………………………65
4.5 Conclusion……………………………………………………………………...66
References…………………………………………………………………………..68
Figures……………………………………………………………………………70

Chapter 5: Hard Disk Top Layer Analysis by Total Reflection X-ray Photoelectron Spectroscopy (TRXPS): Effect of Acetone Rinsing ……...….81
5.1 Introduction……………………………………………………………………81
5.2 Experimental……………………………………………………………………83
5.3 Results and discussion…………………………………………………………84
5.5 Conclusion……………………………………………………………………...85
References…………………………………………………………………………..86
Figures……………………………………………………………………………...88

Chapter 6: Extrinsic and intrinsic contributions to XPS plasmon peaks…...91
References…………………………………………………………………………..95
Figures……………………………………………………………………………...96

Chapter 7: X-ray photoelectron-induced surface plasmon spectroscopy at grazing emission…………………………………………...……………..103

7.1 Introduction……………………………………………..……………..103
7.2 Experiment……………………………………………..……………...104
7.3 Results and discussions……………………………………………………..105
7.4 Conclusions……………………………………………………….………...106
References……………………………………………...……………107
Figures………………………………………………………………………108

Chapter 8: Conclusions……………………………………………………111

Chapter1: Grazing Emission X-ray Analysis: A review

Abstract:

Grazing emission X-ray analysis is a technique of detecting emitted X-rays at very small exit angles. It includes grazing exit X-ray fluorescence analysis (GE-XRF), grazing exit electron probe microanalysis (GE-EPMA), and reflection high energy diffraction–total reflection angle X-ray spectroscopy (RHEED-TRAX). It has been demonstrated that GE-XRF is useful for surface, thin-film and particle analyses. In this method only emitted X-ray fluorescence from small angles is detected, the sample is irradiated at normal incidence or can be double sensitive if irradiated at grazing incidence. It has the advantage of better spatial resolution at longer wavelengths and a larger dynamic range than when the X-ray fluorescence is detected above the critical angle. In the present chapter we give a review of grazing-exit X-ray fluorescnce analysis (GE-XRF) and reflection high energy diffraction (RHEED). Principles and applications are reviewed in this chapter. Setbacks and advantages of the techniques are presented throughout the text. RHEED is explained in two alignments, RHEED-TRAX (Reflection high energy diffraction-Total reflection angle X-ray spectroscopy) where the elctron beam is hitting the sample at a grazing angle and X-rays are detected at grazing exit, and also the normal RHEED where the electron beam is irradiating the sample at approximately normal incidence. X-ray refracted fluorescence (RXF), with the refraction effect of the scattered X-ray fluorescence as the origin of radiation, has been discussed among other two types of instruments.

1.1 Introduction:

Tsuji published a review [1] describing a commercially available SEM experiment and discussing grazing exit electron probe microanalysis (GE-EPMA). His review shows that grazing-exit electron probe X-ray microanalysis is useful in improving the lateral resolution of the sample surface. In addition; the study demonstrated that grazing-exit electron probe X-ray microanalysis can be applied for surface, thin-film, and particle analyses. Electron probe microanalysis (EPMA) is used in

conjunction with SEM and is not generally a surface science technique. It occurs when an electron beam strikes the surface of a conducting sample. The energy of the beam is typically in the range 10-20keV. This causes X-rays to be emitted from the point the material. The energy of the X-rays emitted depend on the material under examination. The X-rays are generated in a region about 2 microns in depth, and thus energy dispersive (EDX) is not a surface sensitive technique. However, by moving the electron beam across the material an image of each element in the sample can be acquired. Measuring X-rays at very small take off angles from the sample can make EPMA applicable in surface sensitive anslysis. This arrangement enables measurement of only the characteristic X-rays emitted from the near surface regions. Due to strong X-ray absorption in the sample and refraction effects at the sample surface, the X-rays emitted from the deep regions are not detected by the EDX detector. Although the intensity of the detected characteristic X-rays is weak by GE-EPMA, GE-EPMA greatly enhances surface sensitivity in X-ray measurement. Tsuji also showed in his review that the probing depth is as shallow as few nanometers at angles below the critical angle of a sample.

Since the observation depth changes drastically with the exit angle, the accuracy is controlled within less than 0.01^{o}. The sample can be tilted to a fixed EDX but the sample stage in a commercially available EMPA does not provide tilting accuracy, the minimum step is usually $>0.5^{o}$. This problem is solved as shown by Tsuji by a motor controller and a computer; the minimum accuracy in such a case is $>0.018^{o}$. To restrict the solid angle for detection, a slit was attached to the top

of the EDX detector; laboratory-made slit system, which was designed for the EDX detector (Ultra mini cup, EX-541-40MU, JEOL) in the commercially available SEM (JSM-5500, JEOL). The EPMA set up can also be moved on a rail. Chapter 2 in this thesis presents an alternative method to the motor controller. In the proposed method, no angle scan mechanism is needed.

Tsuji then explained about the calculation of characteristic X-ray intensity in GE-EMPA. In the calculations, two procedures are required; 1) calculation of the electron reduced X-ray intensity as a function of depth and 2) calculation of the X-ray intensity at grazing exit angles. The depth distribution of generated X-rays is calculated by a Monte Carlo method. In calculations of emissions at grazing angles, refraction and reflection should be considered. Reciprocity theorem was also emphasized in the review stating that the intensities of X-rays emitted at depth Z and observed at a grazing exit angle, are proportional to the X-ray intensities impinging at the same grazing incident angle and produced at depth Z. Comparing GE-EPMA with the program calculations, thickness and density are evaluated. The analytical characteristics of GE-EPMA have been also reviewed by Tsuji in his paper. Lateral broadening is more in the deep regions than near the surface; electrons do not broaden very much near the surface though it depends on the material. GE-EPMA drastically improves the spatial resolution (> 10 times) although the matrix samples can have a clear effect. No restrictions in GE-EPMA for the electron beam size because even if the electron beam size irradiates the substrate beneath the particle and generates X-rays, those X-rays are not detected with the grazing-exit condition, i.e. low background. However, signal to

background ratio is still sufficient to make surface analysis. Sample flatness is reviewed as not a serious problem in gazing exit analysis if the excitation beam is small. The review also discussed examples of applications of GE-EPMA in surface contamination analysis, thin film analysis, particle analysis and analysis of inclusion. A review of fulfilling Tsuji's paper is presented in this work. This chapter considers a comparison between different excitation probes in grazing emission X-ray analysis namely, GEXRF and RHEED. This review is meant to be more inclusive than Tsuji's study in terms of references.

1.2 Principles:

Becker *et al.* [2] pointed out that X-ray fluorescence analysis can be made surface-sensitive not only by grazing-incidence, but also by grazing-emission X-ray fluorescence (GEXRF) techniques. To demonstrate the equivalence between the two geometries, they used the principle of microscopic reversibility which states that grazing incidence and grazing emission type experiments provide identical results if the energies of interest are the same. If this condition is satisfied the depth distributions of atoms contributing to the measured fluorescence are identical. The energy of interest for grazing incidence setups is the primary X-ray beam energy, whereas for grazing exit experiments it is the one of the measured X-ray fluorescence line. Since the latter has a lower energy than the beam energy, grazing emission type experiments are generally more sensitive to absorption of than reflection and refraction X-rays. The optical reciprocity

theorem by Helmhotz, allowing the expectation for an inverted setup of grazing incidence XRF, has been demonstrated applicable in their work [2].

GE-XRF and total reflection X-ray fluorescence (TXRF) [3] are similar in that in both only the fluorescence of atoms near to the interface is observed. Similar information i.e. composition, thickness and density of layers can be obtained from (variable angle) TXRF and GE-XRF. In TXRF, an evanescent or exponentially damped wave exits under the total reflection that penetrates a short distance i.e. about 3 nm. In the optically dense medium, a standing wave field is set up externally as a result of the interference of the incident and reflected waves. So atoms just above or just below the interface can be ejected by the standing wave field or the evanescent wave, respectively. Hence the amount of radiation from the bulk (spectral background) is extremely small owing to the very shallow penetration of the evanescent wave, very low detection limits can be obtained for trace amounts of elements on optically flat substrates. For multilayers, standing wave patterns can be generated inside the layer system. The composition, density and thickness of the layers can be inferred from the angular dependence of the X-ray fluorescence. In GE-XRF, the picture is a little different. Understating the angular dependence of the fluorescence intensity at the air/vacuum side of the optical interface is an essential concept in GE-XRF. Since total reflection does not occur for plane waves incident on the boundary from the optically less dense medium, Fresnel's equations are used describe emission, refraction and reflection that take place for a source sufficiently far removed from the interface and hence

a completely inaccessible region for external emission below the critical angle is found.

Therefore, radiation generated in the bulk of the sample scattered background reach a detector positioned at an angled smaller than the critical angle, though small amounts of characteristic radiation from the bulk material emitted at angles smaller than the critical angle are really observed. This can be due to Fourier decomposition of the emitted spherical waves. For fluorescing atoms very near to the interface (about 3 nm.), Fourier compositions contain evanescent wave components of non-negligible amplitude. Evanescent wave emission at angles smaller than the critical angle is therefore observed in GE-XRF, while it is evanescent wave absorption in TXRF. To find the angular dependence of the emitted fluorescence of the whole sample, the contributions of all individual atoms are added.

For a homogeneous layer, integration over the depth coordinates yields to:

$$I(\theta) = S(\theta).|t(\theta)|^2.\int_0^d \exp\left[-2k\,\mathrm{Im}\sqrt{n^2-\cos^2(\theta).z}\right]\times\left[1+\{multiple.reflections\}\right].f(z)dz$$

where $S(\theta)$ is the instrumental factor and $t(\theta)$ is the transmission factor coefficient at emission angle θ, $k=\frac{2\pi}{\lambda}$ is the wave number, n is the complex refractive index *f(z)* and is the source strength at depth *z*, which is proportional to the concentration at depth *z*. Because *n* depends on the concentrations and hence on *f*, the dependence of *I* on *f* is nonlinear.

So in the TXRF method, the shape of the curve describing the angular dependence of the fluorescence intensity is determined by the wavelength of the incident

radiation, it is therefore the same for all elements in the sample layer. While in GE-XRF, the shape of the spectra of the curve is determined by the wavelengths of the emitted characteristic radiation and hence different for all elements and all lines. GE-XRF spectra therefore contain more information than TXRF.

GE-XRF found a wide range of applications in surface and ultratrace elemental analysis. It has been demonstrated that GE-XRF has the potential for ultra trace analysis of liquid samples [4]. GE-XRF has also been proven a good technique in organic matrices [5] , detection limits for a low-Z element (Na), a medium-Z element (Zn) and a heavy-Z element (Pb) were found 0.4, 1.5 and 2 ng respectively. It has been proven that GEXRF can also be used in pigments [6]. Although GE-XRF is reported time consuming analysing pigments, it could achieve detection of low-Z elements in the pigments. Claes *et al.* [7] reviewed several other applications of GE-XRF in Ref.7. Noma *et al.* [8] demonstrated the principle of reversibility in case of multilayers. The exit angular dependence of the X-ray fluorescence intensity of a Cr/Au layered thin film clearly shows an oscillation structure that represnts the interference of emitted X-rays. Noma *et al.* obtained results in good agreement with those by grazing incidence. Other grazing exit studies for multilayer analysis were also conducted [9-16]. X-ray fluorescence of layered materials is also reviewed by de Boer [17]. Although Kayser *et al* . [18] suggested that X-ray fluorescnce in grazing exit is more sensitive than grazing incidence in this case, we wonder if the area illuminated by X-rays and intensity of both have been taken into account.

Contrary to TXRF, GE-XRF can also be combined with a wavelength dispersive X-ray fluorescence (WD-XRF) leading to improved spectral resolution for light elements in comparison with energy dispersive X-ray fluorescence (ED-XRF). ED-XRF provides simultaneous determination of elements, rapid analysis compared to WD-XRF but it lacks sufficient sensitivity for elements lighter than chlorine and may have some matrix effects while WD-XRF provides better resolution, allows assessment of more elements due to sequential accumulation of spectral lines, lower detection limits and permits measurement of very light and heavy elements basically from Be to U. Both detection techniques are non-destructive and multi-elemental with a detection limit (1-10) μg/g [19,20].

Due to the energy dispersive detection system, TXRF suffers from a limited dynamic range and a poor spectral resolution. These problems may cause some elements not to be detected due to X-ray line overlap. Low atomic number elements are difficult to detect by EDX. The SiLi detector is also often protected by a Be window. The absorption of the soft X-rays by the Be precludes the detection of elements below an atomic number of 11 (Na). In windowless systems, elements with as a low atomic number as 4 (Be) have been detected, but the problems involved get progressively worse as the atomic number is less. The use of the wavelength dispersive detector (WDX) is not justified to solve problems owing to intenisty limitations. Too much intensity is inherently lost when not only the exciting radiation is collimated to a few minutes of a degree but also when the emerging beam is, as required in a wavelenght dispersive detection system, and therfore TXRF can never be combined with WD-XRF where much characteristic

X-ray intensity is lost in dispersion detection limits. GE-XRF serves the solution for this problem. In 1983, Becker *et al.* reported that XRF can be surface sensitive at grazing exit, by detecting X-ray flourescence intensity at grazing exit. The small solid angle of detection is compensated for by irradiating the sample directly with the uncollimated polychromatic radiation from the X-ray tube. GE-XRF is then taking the advantage of total reflection and wavelength dispersion leading to a better resolution and sensitivity for light elements compared to EDXRF. The angular dependence of X-ray fluorescence intensities is explained in a review by de Boer [21] and others [22-26]. Since X-rays emitted from the deep regions are not detected by energy dispersive detectors EDX due to absorption and refraction effects in the sample surface, ED-XRF can also be used in GE-XRF but at the expense of resolution. Fig.1 shows the difference bewteen TXRF and GE-XRF setups.

1.3 Reflection high energy diffraction (RHEED):

In the RHEED, X-rays are detected at grazing exits though incidence can be direct or glancing incidence. This technique uses a primary beam of RHEED (reflection high energy diffraction) as the excitation probe. Swell *et al.* [27-30] and Ino *et al.* [31,32] showed that it is possible to detect an adsorbate of less than one monolayer by measuring X-rays excited by the primary beam of RHEED during the RHEED observations. This technique is far more sensitive to surfaces than usual X-ray microanalysis because the glancing angle of the primary electron beam with respect to the surface is small ($<5^o$) that the beam does not penetrate

into the crystal so deeply. Therefore, the region of X-ray emission is restricted to within several ten nanometers below the surface. When a primary electron beam is incident on the sample on the crystal surface at a small glancing angle, the electrons are scattered in two directions, i.e. towards the outside and towards the interior, by atoms in the surface layers. The electrons scattered towards the outside probably leave the crystal to the vacuum and a small part of the electrons are scattered again towards the interior. On the other hand, many electrons scattered towards the interior in the first stage are scattered towards the vacuum while traveling in the crystal. Consequently, this scattering decreases the number of electrons proceeding to the interior. That is, the distribution of the scattered electrons has a tendency to be bound near the surface by successive scattering. This behavior is expected to be caused also by further scattering, and the distribution is confined nearer to the surface. This is a special effect for a small glancing angle of incidence and differs from vertical incidence as in the normal X-ray micro-analyzer. Therefore the diffusion range of the scattered electrons in the RHEED experiment is small, forming a lens-like region, where the dotted line shows the same region but when the diameter of the electron beam is sufficiently large compared with the penetration depth, the diffusion range of the electrons may become as illustrated in the Fig2.

This technique has the following characteristics; First, RHEED observations and chemical analysis of the same place on the surface can be done simultaneously, because the incident RHEED beam is used to excite fluorescent X-rays. This can

also be done using reflection high energy diffraction -Auger electron spectroscopy (RHEED-AES) system. Second, this technique is suitable for investigating surface layers from 0.02 Å to 100 Å in depth. Third, operation of the technique is very easy, because the setting-up sample and the apparatus are very simple. A comparison between RHEED and LEED (Low Energy Electron Diffraction) is done by Ino *et al.* [32]. X-rays are mostly emitted in RHEED.

This method is therefore useful for the in situ observation of surface phenomena. It may be especially powerful for the investigation of film growth whose thickness ranges from 0.02 Å to 100 Å. Hasegawa, also known for outstanding research in STM [33]; presented with others for the first time reflection high energy diffraction-total reflection angle X-ray spectroscopy (RHEED-TRAX) [34]. They reported that when the X-ray exit angle is set small and corresponding for the critical angle for total reflection of the marked characteristic x-ray, the surface sensitivity of this X-ray spectroscopy becomes several score times as high as reported by Ino *et al.* [32] (RHEED-TRAX) is comparable of Auger electron spectroscopy AES in general and superior to it for the detection of heavier elements on surfaces. Hasegawa *et al.* demonstrated this enhancement of surface sensitivity with Ag on Si (111). Fig 3 shows the alignment of (RHEED-TRAX).

The information obtained by this method is affected by the experimental conditions, such as the beam energy E_o, the glancing angle, the azimuthal angle of the incident electron beam with respect to the crystal orientation of the substrate

and the take-off angle of the emitted X-rays with respect to the surface. (Fig.4) shows the θ_t dependence of the X-ray spectra taken from a Si (111) surface onto which a monolayer of Ag was deposited at room temperature. The energy of the primary beam was 15 keV and the glancing angle was 3.7^o. When θ_t is set to 2.6^o, the intensity of the Si K_α line (1.74 keV), which comes from the Si substrate, is very strong compared with that of Ag L_α (2.99 keV) and Ag L_β (3.15 keV) lines are emitted from the deposited Ag atoms. At θ_t = 0.6 ^{o}, however, Ag L_α line stands out from the fluctuation of the background continuous X-ray so clearly that the peak to background ration increases about seven times more than that at 2.6^o. Hence, one can detect an extremely small quantity of Ag on the surface with much higher sensitivity at this take-off angle of Ag L_α line is comparable to less than θ_t =2.6^o. When θ_t is less than 0.6^o, the intensity of Ag L_α line is comparable to that of Si K_α line and the shape of the continuous X-ray spectra varies markedly with θ_t [35, 36].

In (Fig.5), the θ_t dependence of the absolute intensities (peak heights) of Ag L_α and Si K_α line is shown. With the increase of θ_t, the intensity of the Ag L_α line increases rapidly and takes a maximum value at θ_t =0.6^o, and then decreases to a smaller constant value. In contrast, the intensity curve of the Si K_α line bends sharply at θ_t= 1.0^o and then gradually increases as θ_t becomes larger than 1.0 ^{o}. The Ag L_α intensity shows a strong peak, but the Si K_α line intensity is shown at each critical angle for total reflection. The relative intensity of the Ag L_α line to the Si K_α, which indicates the intensity ratio of the signal from the topmost layer

of the surface to that from the topmost layer of the surface to that from the substrate Si crystal below the Ag film, is an index of the surface sensitivity of this detection method. So it can be said that the surface sensitivity varies with θ_t and is highest around $\theta_t = 0.3^o$.

The reason the intensities of the characteristic X-rays emitted from the deposited film and the substrate vary with the X-ray take-off angle θ_t in this way can be explained as follows; since the refractive index of materials for X-rays is slightly less than unity, the X-ray emitted from the inner bulk refracts at the surface. Since the Si K_α line is emitted from the region ranging from the surface to the inner bulk crystal, the features of the intensity curves of Si K_α line versus θ_t in is understood by integrating the X-ray intensity emitted at each depth layer, taking into account the absorption effect of both the primary electron beam and the emitted X-ray in the material, and the refraction at the surface.

The reason for the enhancement of the surface sensitivity is considered as follows; X-rays are emitted from the atoms in the topmost layer in a direction parallel to the surface, if the X-ray detector is set at the critical angle θ_c for total reflection, we can detect the X-rays emitted only from the atoms near the surface. This preferential detection of only the surface atoms may be furthered when θ_c is set between 0° and θ_c because of the absorption effect of X-rays. In this condition, furthermore, when θ_c of the characteristic X-ray from the substrate is larger than that of the deposit X-ray scarcely reaches the detector. And, since θ_c is usually very small, the continuous background X-rays of the same energy as the marked characteristic line from the deposit, which come from the deeper bulk, are weak

because of the absorption effect in the sample. Under these conditions, the S/N ratio (or peak to background ratio) of the detection of the surfaces increases drastically to become comparable to AES.

This X-ray technique is not only effective for chemical analysis of the topmost atoms, but also of the deeper region from the surface. Moreover, in the RHEED-TRAX the position and periodicity of atomic arrangement of the same area can be simultaneously examined. The X-ray spectra can be easily measured during the deposition onto the surface or during the desorption from the surface without interrupting RHEED observation. These features remarkably contrast with LEED-AES (Low Energy Electron Diffraction- Auger Electron spectroscopy). RHEED-TRAX is thus an effective technique for the chemical analysis of solid surfaces, and especially favorable MBE (molecular beam epitaxy) and the analytical electron microscope.

Compared to X-ray microanalysis (XMA), when the X-rays are measured in the total reflection angle X-ray spectroscopy TRAX condition, X-rays from the bulk do not reach the detector and only X-rays from the surface region can be detected. Under the usual X-ray microanalysis (XMA), X-rays from several atomic layers below the surface are swamped by the intense X-rays from the inner bulk region. Moreover, in the RHEED-TRAXS, since the primary electron beam irradiates the sample at a grazing angle, the excitation efficiency of X-rays in surface region becomes much higher than the usual XMA. The RHEED-TRAXS and AES are

thought to differ from each other in the nature of the obtained information, which is mainly originated in the differing sampling region near the surface. Because the escape depth of Auger electrons is usually about 5 to 30 nm from the surface, AES is useful for the chemical analysis of a few surface layers.

Other properties of RHEED-TRAXS which in general contrast with AES are as follows:

(1) Unlike the LEED-AES method, since it is the primary electron beam of RHEED that excites the X-rays which are detected, this method can carry out a localized observation of atomic arrangement and chemical analysis of the same surface area. (2) This X-ray spectroscopy may be more favorable for quantitative chemical analysis than AES. The secondary electrons and the inelastically scattered electrons constitute a higher background in AES measurements compared with the X-ray spectroscopy. Moreover, because of the extremely small escape depth of Auger electrons, the intensity attenuation of emitted Auger electrons in the sample is highly affected by various factors such as multiple scattering, surface roughness and aggregation states of atoms, etc. Although these factors make a quantitative analysis difficult in the case of AES, the X-ray measurement in RHEED-TRAXS may be scarcely affected by these phenomena because of their high energies and extremely small interaction with matters. (3) This X-ray spectroscopy is available not only for the chemical analysis of the topmost atomic layer on the surface but also for a deeper region below the surface. That is, by making the X-ray take-off angle larger and keeping away from the angle region of total reflection, the X-rays from the deeper region also reach the

detector. The detection depth below the surface becomes several hundred angstroms. (4) The X-ray emission is a competing relaxation process of ionized atoms with the emission of Auger electrons, and its ratio grows larger as the atomic number increases. So RHEED-TRAXS is more favorable for the detection of heavier atoms.

RHEED-TRAXS has, on the other hand, the following shortcomings: (1) Because the critical angles of total reflection of X-rays are in general small, in order to obtain a sharp enhancement of the intensity of the marked characteristic X-rays by the refraction effect, one must control the take-off angle very accurately and prepare a very flat surface on a nearly atomic scale. But it is rather difficult, because the take-off angle easily changes by a slight distortion of the surface. A slight distortion and slip bands of Si wafers caused by heat-treatment of the samples affected the X-ray intensities was observed. (2) The data acquisition in the RHEED-TRAX apparatus is less prompt than in the case of the usual AES system. In order to reduce the statistical error, it takes about one minute or more to accumulate the data for one spectrum.

A study comparing RHEED-TRAX and AES X-ray spectroscopy in Si(111)-Ag system was carried out by Hasegawa *et. al.* [37]. In their study, the RHEED-TRAX method was applied to the isothermal condensation and desorption experiments of Ag atoms, saturation coverage of surface structures and desorption energies of Ag atoms was measured. The sticking probability and the desorption rate of Ag atoms was directly measured by RHEED-TRAXS experiment and

compared with results obtained by AES. Other studies have investigated the crystal growth by RHEED-TRAX [38-47]. Grazing spectroscopies for X-ray emission is also done with particle induced X-ray emission (PIXE). The first such experiment employed a modification to the conventional PIXE technique wherein characteristic X-rays for a low-Z surface adsorbate (at the monolayer concentration level) was obtained at grazing exits. Due to possibility of beam-induced damage to fragile or weakly-bonded surface species, Rodirguez-Fernandez *et al.* [48] used an unperturbed detector in direct contrast to the small acceptance angles used in XRF for the measurement of low surface coverage of Sulphur on InP(001). Refraction and reflection effects at grazing geometries, for incident electrons and photons, were not attempted. Van Kan *et. al.* [49] attempted grazing incident angle PIXE (also known as TPIXE, or total reflection PIXE) using thin Au layers on a quartz substrate with some success, in his work he suggests that grazing exit is more sensitive than grazing incidence. The main obstacle determining monolayer overages on thick substrates arises from the intense X-ray signal emanating from the substrate. Substrate X-ray yields could be attenuated by observing X-ray radiation emitted at rather grazing emergence, whereby the photons will be substantially attenuated by the substrate atoms themselves. PIXE shows 1) better resolution that ED-XRF though at energies lower than 20 keV, better energy resolution full width at half maximum (FHWM) is achieved with wavelength dispersive fluorescence (WD-XRF) as compared to PIXE and energy dispersive fluorescence (ED-XRF). While the FWHM using Si(Li) detector is 160 eV, it is less than 10 eV for WDXRF at 5.9 keV. Depending

on the collimator (fine/ extra-fine) and order of diffraction (first/second), the FWHM varies from 10 eV to 50 eV for LiF (220) crystal and form 10 eV to 70 eV for LiF (200) crystal at about 12 keV. However, the energy resolution with LiF (200) crystal is approximately equal to that of a Si(Li) detector system at energies around 20 keV. 2) Less penetration depth and less analytical volume (about 10-50 micrometer) even when applied to thick samples. 3) ED-XRF is a better technique for the determination of elements with low energy lines which fall especially in the range of 1-4 keV (Na through Ca), while PIXE is better for elements with relatively higher characteristic X-ray energies. For elements with atomic number greater than (or about 50), both techniques are forced to use L X-ray lines in place of K X-ray lines. 4) Compared to XRF, the detection limit by PIXE is better by one order of magnitude. 5) PIXE is less flexible in regards of detectors and excitation sources but there is flexibility in choice of ion type, beam energy, sample support, and considerable flexibility in changing the geometry of the system [50-54].

1.4 Comparison between ED-XRF and WD-XRF Techniques in GE-XRF:

1.4.1 Resolution

The lower the resolution, the more easily an elemental line is distinguished from other nearby X-ray line. The resolution of the WD-XRF system, which is dependant on the crystal and optics design, particularly collimation, spacing and positional reproducibility, varies from 2 to 10 eV at 5.9 keV. While the resolution in WD-XRF depends on the diffracting crystal, the resolution of the EDX system

is dependent on the resolution of the detector. This can vary from 150–200 eV for Si(Li) and HpGe and about 600 eV or more for gas filled proportional counter at 5.9 keV.

1.4.2 Simultaneity

ED-XRF has the capability to detect a group of elements all at once while it is not possible with the WD-XRF system.

1.4.3 Spectral Overlaps

Since the resolution of a WD-XRF spectrometer is relatively high, spectral overlap corrections are not required. However, with the ED-XRF analyzer, a de-convolution method must be used to correct for spectral overlaps as it has poor resolution. The spectral de-convolution routines however, introduce error due to counting statistics for every overlap correction onto every other element being corrected for. This can double or triple the error.

1.4.4 Background

The background radiation is one limiting factor for determining detection limits, repeatability, and reproducibility. Since a WD-XRF system usually uses direct radiation flux, the background in the region of interest is directly related to the amount of continuum radiation. However, the ED-XRF system uses filters and/or targets to reduce the amount of continuum radiation in the region of interest, which is also resolution dependant, while producing a higher intensity X-ray peak

to excite the element of interest. Thus although the WD-XRF has an advantage due to resolution, yet it suffers a large background i.e., if a peak is one tenth as wide, it has one tenth the background.

However, ED-XRF counters with filters and targets can reduce the background intensities by a factor of ten or more.

1.4.5 Excitation Efficiency

Excitation efficiency is the main factor for determining detection limits, repeatability, and reproducibility. The relative excitation efficiency is improved by having more source X-rays closer to but above the absorption edge energy for the element of interest. WD-XRF generally uses direct unaltered X-ray excitation, which contains a continuum of energies with most of them not optimal for exciting the element of interest. However, ED-XRF analyzers may use filter to reduce the continuum energies at the elemental lines, and effectively increase the percentage of X-rays above the element absorption edge.

A strong point of WD-GEXRF is the determination of light elements with low detection limits. Given the prototype status of this grazing emission technique, the detection limits for light elements (sub-nanogram level) obtained for environmental sample analysis can probably be improved. It can be stated that WD-GEXRF is a promising technique for the determination of light element contamination on silicon wafers. Detection limits in the high 10^{10} at cm^{-2} region for K and Ca have been reported and it is expected that both instrumental

developments and the use of pre-concentration steps can improve these values. It has been demonstrated that the detailed performance of layer analysis with GE-XRF can support process control. However, the main drawbacks of this WD-GE-XRF technique are the prohibitively time-consuming aspect when many elements have to be determined and the limited linear dynamic range due to matrix effects, especially for environmental trace element analysis. The energy-dispersive detection variant of the grazing emission technique has already proven its efficiency in the analysis of surface layers, while the probe depth variations of structured samples were easily performed with WD grazing emission soft x-ray spectroscopy [55-57].

1.5 RXF (X-ray refracted fluorescence) in GE-XRF:

The angular distribution of X-ray fluorescence is an anisotropic radiation, with the refraction effect of the scattered X-ray fluorescence as the origin of radiation. This effect can be utilized in surface and interface analysis. 1) Surface density, 2) Chemical condition of the sample substrate i.e. oxidation, reduction, etc…., 3) Interface roughness and 4) The particle diameter of elements on the sample surface; can be obtained by this technique. The possibility of surface analysis by the refraction dispersive system (RDS) was for the first time demonstrated by Sasaki *et. al.* [58-66].

GE-XRF was applied to elemental analysis in chemical microchips; a good relation between the X-ray fluorescence intensities and concentrations of standard solutions was obtained and the XRF background was reduced [67]. GE-XRF has

also been applied to analysis of hazardous metals attached to a plant leaf surface using an X-ray absorber Method [68]. Soft X-ray emission allows chemical state information to be obtained owing to the high spectral resolution and the small lifetime broadening [69]. Weak X-ray sources can be used to study probing depth or the chemical composition in a similar way in X-ray reflectometry (XRR) [70] or total X-ray reflection fluorescence (TXRF) [71,72]. Synchrotron radiation is also used in gazing exit emission for refined spectra [73-76].

1.6 Assessment of instrument:

Several GE-XRF devices have been constructed independently at Tohoku University, Japan [59], Philips Research Laboratories in Eindhoven, the Netherlands [57] and at Cordoba National University, Argentina [58]. The GE-XRF instrument designed at Tohoku University by Sasaki *et al.* [59] is above-discussed. Both of the other two instruments use PW2400 WD-XRF and the difference between them is the application of a double-slit system. In the Philips Research Laboratories in Eindhoven, the Netherlands by de Bokx *et al*. [49], two invariable slits are used making it advantageous in two ways: 1) It makes the FWHM narrower because the slit resolution is not less by non-collimated beam of primary X-rays since fluorescence is unidirectional; 2) The FWHM is fully determined by the inherent resolution of a multilayer, without any contribution of the rigid slit system and other parts of the instrument. The contribution of the spatial resolution of the slit is noticeable. For the other instrument constructed at Cordoba National University, Argentina by Perez *et al.* [58], two adjustable

slits ,allowing a better collection of fluorescent X-rays much higher quantum efficiency, 2 orders of magnitude lower detection limits; are used.

Beside the ED-XRF common disadvantages, GE-XRF instruments are worsened in general by two additional points [77, 78]. 1) The first is the application of a conventional Rh end window tube. By using such a tube the average direction of excitation (= 62° +θ, θ is the grazing exit angle) is not perpendicular in relation to the sample surface and increases the background, thus spoiling the low detection limits. This conclusion is strongly supported by the most recent results of an inter-instrumental, inter-laboratory study of drinking water samples. 2) Real samples, which can be normally analyzed by grazing angle methods, show all kinds of inconsistencies and differ highly from the model samples assumed for the theoretical description. Their surfaces are rough and much different from at uniform plates ideally demanded for total refection methods. Furthermore they do not show regular, periodic patterns, which are relatively easy to trace. Although there have been efforts to analyse rough surfaces by use of similar techniques, and to derive the sample density, thickness, or period and roughness from the critical angle, fringe distance, amplitude values of real spectra, the problem is still far from being solved.

Similar problems plague the TXRF technique as well, but are less important for quantitative analysis. Simply, for shorter X-ray wavelengths, characteristic for medium- and high-Z elements, the chemical and topographical influences are less serious than for long wavelength GE-XRF.

1.7 Concluding Remarks:

Grazing emission X-ray analysis has been presented in terms of priciples and applications with emaphsis on reflection high energy diffraction (RHEED). It was shown that RHEED-TRAX is double-sensitive and assesses both physical and chemical parameters of a sample. It can be applied in surface, thin-film and particle analyses. It is more favorable than AES in quatatitave analysis and heavy atoms but it still has shortcomings since the take-off angle easily changes by a slight distortion of the surface. A slight distortion and slip bands of Si wafers is possible. This effect can be utilized in surface and interface analysis. 1) Surface density, 2) Chemical condition of the sample substrate i.e. oxidation, reduction, etc…., 3) Interface roughness and 4) The particle diameter of elements on the sample surface; can be obtained by this technique. A comparison between two instruments and XRF has been presented. Coupling of both and utilizing XRF one can get 1) better assessment of light elements, at very low concentration levels, 2) identification of stratified layers at extreme cases, 3) density profiling due to its ability to perform multilateral inspection.

References:

1. K. Tsuji, Spectrochim. Acta, Part **B 60** (2005) 1381-1391.
2. R. S. Becker, J. A. Golovchenko, and J. R. Patel, Phys. Rev. Lett. **50** (1983) 153-156.
3. P.K. de Bokx, Chr. Cok, A. Bailleul, G. Wiener, H.P. Urbach, Spectrochim. Acta, Part **B 52** (1997) 829-840.
4. M. Claes, P. K. de Bokx, N. Willard, P. Veny and R. VanGrieken, Spectrochim. Acta, Part **B 52** (1997) 1063-1070.
5. Z. M. Spolnik, M. Claes and R. Van Grieken, Anal. Chim. Acta, **401** (1999) 293-298.
6. M. Claes, R. Van Ham, K. Janssens and R. Van Grieken, Adv.X-Ray Anal. **41** (1999) 262-277.
7. M. Claes, R. van Grieken, and P. K. de Bokx, X-Ray Spectrom. **26** (1997) 153-158.
8. T. Noma, A. Iida and K. Sakurai, Phys. Rev. **B 48** (1993) 17524-17536.
9. M. Iwami, M. Hirai, M. Kusaka, M. Kubota, S. Yamamoto, H. Nakamura, H. Watabe, M. Kawai and H. Soezima, Jpn. J. Appl. Phys. **29** (1990) 1353-1356.
10. G.Wiener, S.J. Kidd, C.A.H. Mutsaer, R.A.M. Wolters, P.K. de Bokx, App. Phys. Sci. **125** (1998) 129-136.
11. T. Noma and Atsuo Iida, J. Synchrotron Rad. **5** (1995) 902-904.
12. F.Pfeiffer, W.Zhang and I. K. Robinson, Appl. Phys. Lett., **84** (2004) 1847-1849.
13. Y. Osada, X-Ray Spectrom. **34** (2005) 92–95.

14. T. Kashiwakura, S. Nakai, Radiat. Phys. Chem. **75** (2006) 1888–1893.

15. H. P. Urbach and P. K. de Bokx, Phys. Rev. **B 63** (2001) 085408-085417.

16. T. Noma,K. Takada1 and A. Iida, X-Ray Spectrom. **28** (1999) 433-439.

17. Y. Kayser, D. Banaś , W. Cao , J.-Cl. Dousse , J. Hoszowska , P. Jagodziński , M. Kavčič ,A. Kubala-Kukuś , S. Nowak , M. Pajek and J. Szlachetko, Spectrochim. Acta, Part **B 65** (2010) 445-449.

18. D.K. G. de Boer, Phys. Rev. **B 35** (1996) 6048-6064.

19. J. Szlachetko, D. Banaś, A. Kubala-Kukuś, M. Pajek, W. Cao, J.-Cl. Dousse,J. Hoszowska, Y. Kayser, M. Szlachetko, M. Kavčič, M. Salome, and J. Susini, J. Appl. Phys. **105** (2009) 086101-086103.

20. D.K. G. de Boer, X-Ray Spectrom. **18** (1989) 119-129.

21. H. Urbach and P. de Boxx, Anal. Sci. **11** (1995) 549-552.

22. H. Urbach and P. de Boxx, Phys. Rev. **B 53** (1996) 3752-3763.

23. P.B. Swell and M. Cohen, Appl. Phys. Lett. **11** (1967) 298-299.

24. S.M.P. Smolders and H.P. Urbach, J. Eng. Math. **43** (2002) 115–134.

25. R. D. Perez, H. J. Sa´ nchez and M. Rubio, X-Ray Spectrom. **31** (2002) 296–299.

26. Aleksandr Bekshaev, Ren´e Van Grieken, Spectrochim. Acta, Part **B 56** (2001) 503-315.

27. P.B. Swell and D.F. Mitchell, J. Appl. Phys. **42** (1071) 5879-5882.

28. D.F. Mitchell and P.B. Swell, Surf. Sci. **55** (1976) 367- 372.

29. D.F. Mitchell, P.B. Sewell and M. Cohen, Surf. Sci. **61** (1976) 355- 376.

30. S. Ino, T. Ichikawa and S. Okada, Jpn. J. Appl. Phys. **19** (1980) 1451-147.

31. S. Ino, J. Phys. Soci. Jpn. **65** (1996), 3248-3253.

32. S. Ino, Jpn. J. Appl. Phys. **16** (1977) L891-L908.

33. S. Hasegawa , I. Shiraki, F. Tanabe and R. Hobara, Curr. Appl. Phys. **2** (2002) 465–471.

34. S. Hasegawa, S. Ino, Y. Yamamoto and H. Daimon, Jpn. J. Appl. Phys. **24** (1985) L387-L390.

35. K. Kimura, M. Hasegawa, and M. Mannami, Phys. Rev. **B36** (1987) 7-11.

36. P.W. Palmberg, Anal. Chem. **45** (1973) A549-&.

37. T.Usui, Y. Aoki, M. Kamei, H. Takahashi, T. Morishta and S. Tanaka, Jpn. J. Appl. Phys. **30** (1991) L2032-L2035.

38. S. Hasegawa, H. Daimon and S. Ino, Surf. Sci. **186** (1987) 138- 62.

39. Y. Yamamoto **,** Surf. Sci. **271** (1992) 407-415.

40. Y. Yamamoto **,** Surf. Sci. **281**(1993) 253-269.

41. Y. Yamamoto, Jpn. J. Appl. Phys. **32** (1992) 2544-2549.

42. Y. Yamamoto, Jpn. J. Appl. Phys. **31** (1992) 2241-2422.

43. Y. Yamamoto, Jpn. J. Appl. Phys. **31** (1992) L53-L56.

44. Y. Yamamoto, S. Kitamura, M. Iwatsuki, Jpn. J. Appl. Phys. **31** (1992) L635-L637.

45. T. Noma, H. Miyata and S. Ino, Jpn. J. Appl. Phys. **31,** (1992) L900.

46. J. Shigetomi, K.Fuwa, S.Shimizu and S. Yamakawa, H. Crys. Growth. **111** (1991) 110-114.

47. I. K. Koshelev, A. P. Paulikas, S. Uran, M. B. Beno, G. Jennings, J. Linton, and B. W. Veal, **59** (2002), 469-481.

48. T. Narusawa, S. Shimizu, S.Komiya, Jpn. J. Appl. Phys. **17** (19782) 721-722.

49. L. Rodriguez-Fernhdez , W.N. Lennard, H. Xia, G.R. Massoumi, Appl. Surf. Sci. **103** (1996) 289-298.

50. J.A. van Kan, R.D. Vis, Spectrochim. Acta, Part **B 52** (1997) 847–853.

51. K. Tsuji, M.Huisman, Z. Spolnik, K. Wagatsuma, Y. Mori, R. E. Van Grieken, R. D. Vis, Spectrochim. Acta, Part **B 55** (2000) 1009-1016.

52. W.N. Lennard, J.K. Kim, L. Rodriguez-Fernhdez, Nucl. Instr. And Meth. In Phys. Res. **B 189** (2002) 49-55.

53. A. Ene, I.V. Popescu and C.Stihi, Ovidius University Annals of Chemistry. **20** (2009) 35-39.

54. V. Vijayan, R. K. Choudhury, B. Mallick, S. Sahu, S. K. Choudhury, H. P. Lenka, T. R. Rautray and P. K. Nayak, CURR SCI INDIA. **85** (2003) 772-777.

55. T.Awane, S.Fukuoka, K.Nakamachi, and K.Tsuji, Anal. Chem. **81** (2009)**,** 3356–3364.

56. M. Claes,P. de Bokx2 and R. Van Grieken**, ,** X-Ray Spectrom. **28** (1999) 224–229.

57. P. de Boxx and H. Urbach, Rev. Sci. Instrum.**66** (1994) 15-19.

58. R.D. Perez and H. J. Sanchez, Rev. Sci. Instrum. **68** (1997) 2681-2684.

59. Y. Sasaki and K. Hirokawa, Appl. Phys. **A 50** (1990) 397-404.

60. S. Sato, K. Tsuji and K. Hirokawa, Appl. Phys. **A 62** (1996) 87-93.

61. Y. Sasaki and K. Hirokawa, Appl. Phys. Lett. **58** (1991) 1384-1386.

62. T. Noma and A. Iida, Rev. Sci. Instrum. **65** (1994) 837-344.

63. Y. Sasaki, Jpn. J. Appl. Phys. **30** (1991) L761-L763.

64. Y. Sasaki, M. Kisimoto, S.Nagata, S.Yamaguchi and K. Hirokawa, Appl. Phys. Lett. **69** (1991) 8420-8422.

65. Y. Sasaki and K. Hirokawa, Appl. Surf. Sci. **47** (1991) 371-374.

66. T. Shoji, K. Hirokawa, Surf. Inter. Anal. **18** (1992) 773-776.

67. K.Tsuji, T.Emoto, Y. Nishida, E. Tamaki, Y. Kikutani, A. Hibara and T. Kitamori, Anal. Sci. **21** (2005) 799-803.

68. T. Awane, S. Fukuoka, K. Nakamachi, and K. Tsuji, Anal. Chem. **81** *(*2009) 3356–3364.

69. P. Skytt. B. Galnander, T. Nyberg, J. Nordgren, P. Isberg, Nucl. Inst. & Methods. Phys. Res. A **384** (1997) 558-562.

70. A.Alshehabi, S. Kunimura and J.Kawai, Anal. Methods. **2** (2010) 1555–1558.

71. S. Kunimura and J. Kawai, Anal. Chem. 79 (2007) 2593-5.

72. P. Willich and R. Bethke, Fresenius. J. Anal. Chern. 353 (1995) 389-92.

73. J. Hoszowska, J.-Cl. Douse, J. Kern, Ch. Rheme, Nucl. Instrum. Methods Phys. Res., Sect. **A 376** (1996) 129-38.

74. T. Noma and A. Iida, Rev. Sci. Instru. **65** (1994) 837-844.

75. A. Kubala-Kukuś, D. Banaś,1 W. Cao, J.-Cl. Dousse, J. Hoszowska,2 Y. Kayser, M. Pajek,1 M. Salomé J. Susini,J. Szlachetko, and M. Szlachetko, Phys. Rev. **B 80** (2009) 113305-113309.

76. F. Meirer, G. Pepponi, C. Streli, P. Wobrauschek, and N. Zoeger, J. Appl. Phys. **105** (2009) 074906-074911.

77. Andrzej Kuczumow, Martine Claes,a Martina Schmeling, ReneÂ Van Griekena and Stefan de Gendt, J. Anal. At. Spectrom. **15 (**2000) 415-421.

78. Andrzej Kuczumow, Martina Schmeling and ReneÂ Van Grieken, J. Anal. At. Spectrom. **15** (2000) 535-542.

Figures

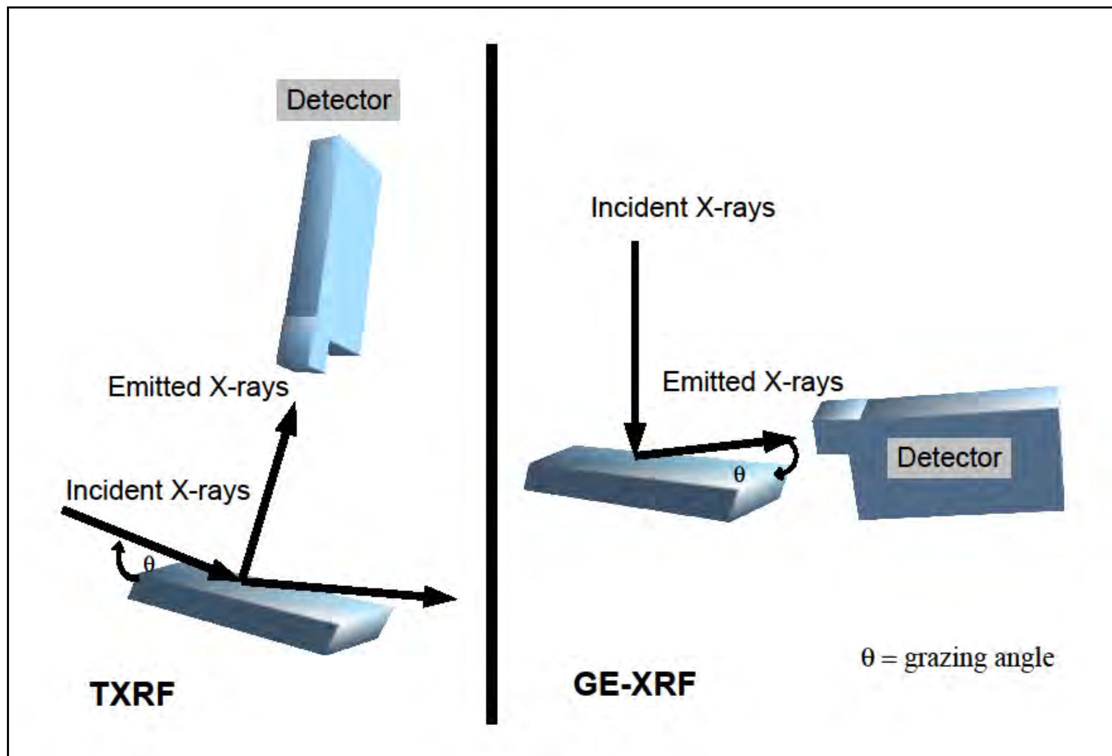

Fig 1: Schematic Illustration of TXRF and GE-XRF geometry.

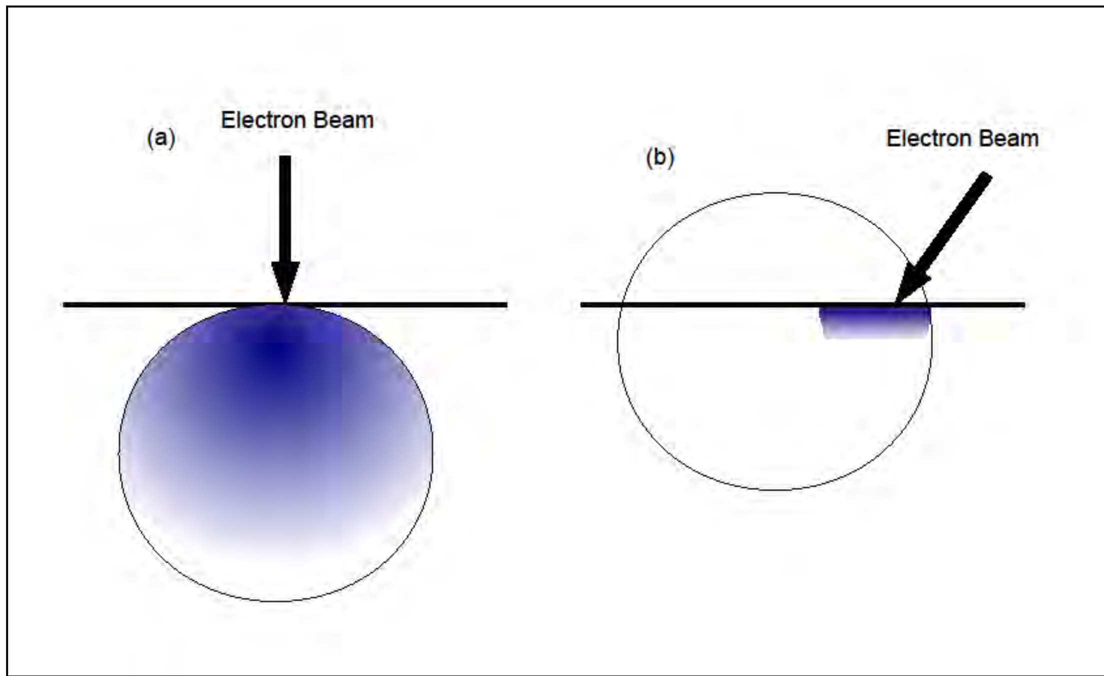

Fig 2: Diffusion range of the electron beam (a) and (b) are the vertical and galncing incidence respectively.

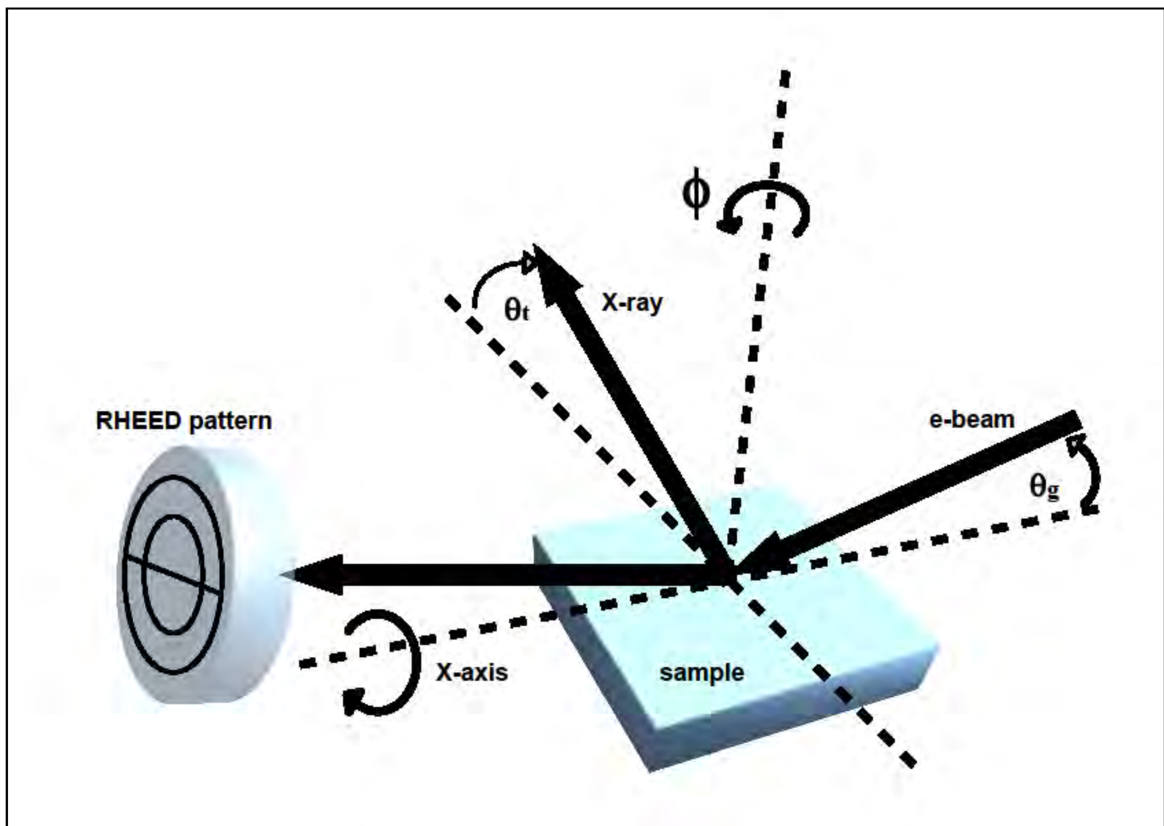

Fig 3: Schematic illustration for the apparatus used for total reflection angle X-ray Spectroscopy in RHEED experiments (RHEED-TRAX).

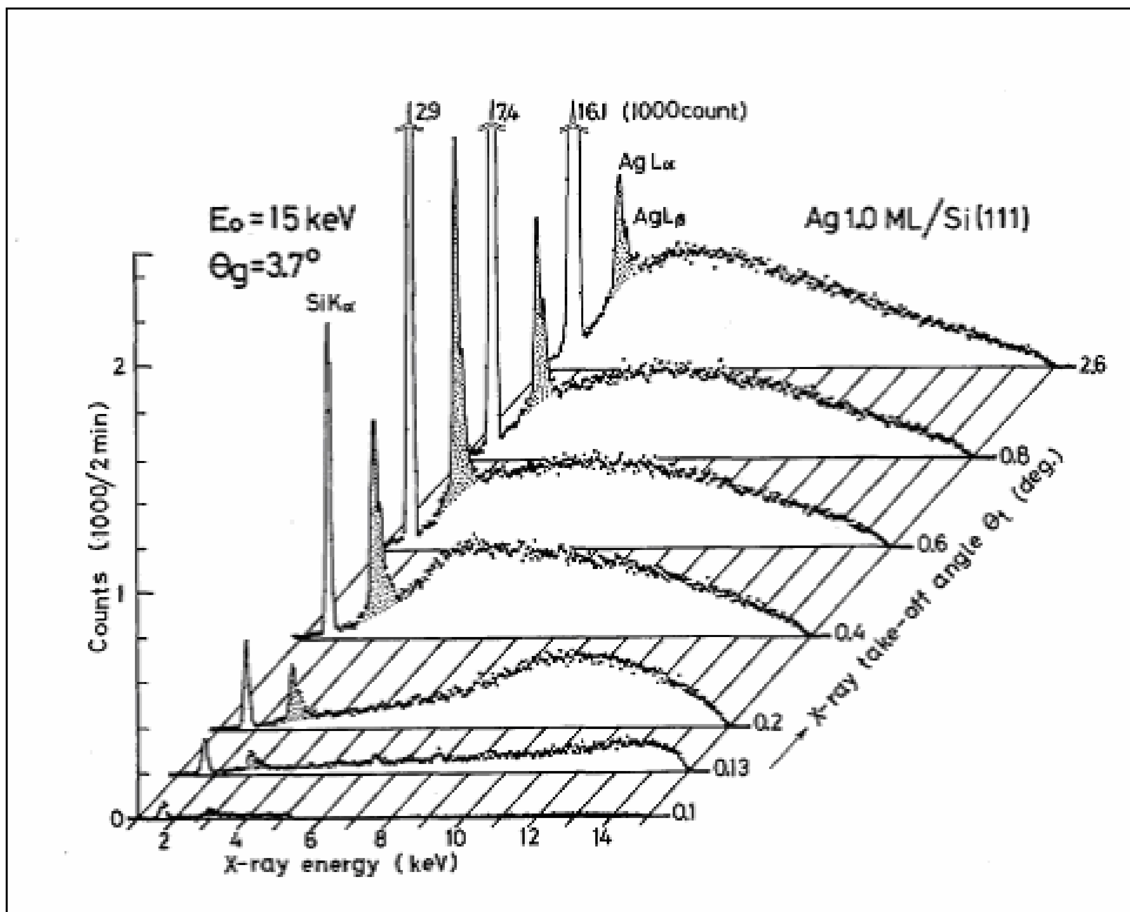

S. Hasegawa, S. Ino, Y. Yamamoto and H. Daimon, Chemical Analysis of Surfaces by Total-Reflection-Angle X-Ray Spectroscopy in RHEED Experiments (RHEED-TRAXS), Jpn. J. Appl. Phys. **24** (1985) pp. L387-L390.

Fig 4: X-ray spectra of (RHEED-TRAX) taken at different take-off angles of the emitted X-ray from Si(111) surface after Ag deposition.

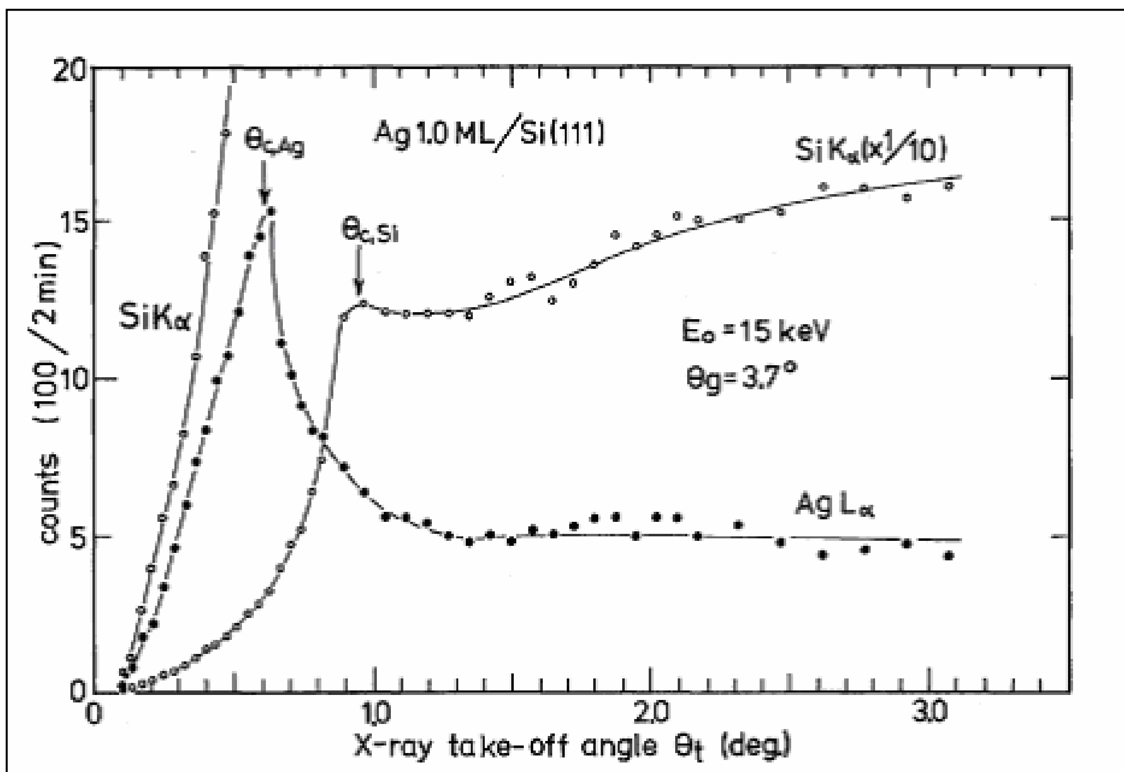

S. Hasegawa, S. Ino, Y. Yamamoto and H. Daimon, Chemical Analysis of Surfaces by Total-Reflection-Angle X-Ray Spectroscopy in RHEED Experiments (RHEED-TRAXS), Jpn. J. Appl. Phys. **24** (1985) pp. L387-L390.

Fig 5: Dependences of absolute intensities (peak heights) of the characteristic X-ray take-off angle.

Chapter 2 :Localised impurity analysis of a 45° inclined sample by grazing-exit SEM-EDX

Abstract :

Impurity in a Cu 45° inclined surface has been analysed and determined. X-rays emitted at grazing and non-grazing angles were compared. The impurity was not burried but on the surface determined by SEM. The impurity was composed of O, Mg and Ca . The X-ray intensity, emitted from a 45° inclined copper surface was found independent of the exit angle.

Angle dependency in grazing-exit SEM-EDX has been successfully demonstrated [1-5] to analyse surface morphology . However the angle scaning mechanism is needed in the high vacuum SEM chamber. We report in this technical note that the use of a 45° inclined surface sample piece makes it possible to measure grazing exit SEM-EDX analysis without using the angle scan mechanism. In the method, a 45° slope surface limits rotation to horizontal; yielding to less-time consuming and more precise measurement compared to other proposed methods [5].

Impurity in a Cu 45° inclined-surface sample has been analysed. Fig1. shows a photo of the model sample with an inclined surface 45°. This was truly a commercially available sample holder for SEM microscope, but the sample piece can be prepared with the same shape to have a 45° inclined-surface. The sample is 8 mm long and 6 mm wide. A SEM (JOEL JSM-5610LVS) was used at 15 kV. Intensity from the impurity was detected at grazing (1°) and non-grazing exits (3°,

5°, 14°). The duration time for measurement was 100 s. The inclusion elements were O, Mg and Ca.

Fig 2. shows the emitted X-ray spectrum. The intensity was found independent of the X-ray exit angle; the same at grazing and non-grazing exit. This is due to the fact that the impurity particle was on the surface. Because X-rays are not only emitted by the impurity itself but by the surrounding copper matrix, other elements can be found.

To summarise, we have measured X-ray intensity emitted at grazing and non-grazing angles of a Cu 45° inclined-surface. Time-consuming detector alignment to grazing exit positions in the conventional method is not needed in the 45° inclined surface method.

References:

1. S. Hasegawa, S. Ino, Y. Yamamoto and H. Daimon, Jpn. J. Appl. Phys. **24** (1985) L387-L390.
2. S. Ino, T. Ichikawa and S. Okada, Jpn. J. Appl. Phys. **19** (1980) 1451-1457.
3. K. Tsuji, Z. Spolnik, T. Ashino, Rev. Sci. Instrum. **72** (2001) 3933– 3936.
4. T. Tetsuoka, T. Nagamura, K. Tsuji, X-Ray Spectrom. **35** (2006) 89-92.
5. K. Tsuji, Grazing-exit X-ray spectrometry, in: K. Tsuji, J. Injuk, R.E. Van Grieken (Eds.), X-Ray Spectrometry: Recent Technological Advances, John Wiley & Sons, Ltd, 2004, pp. 293–305.

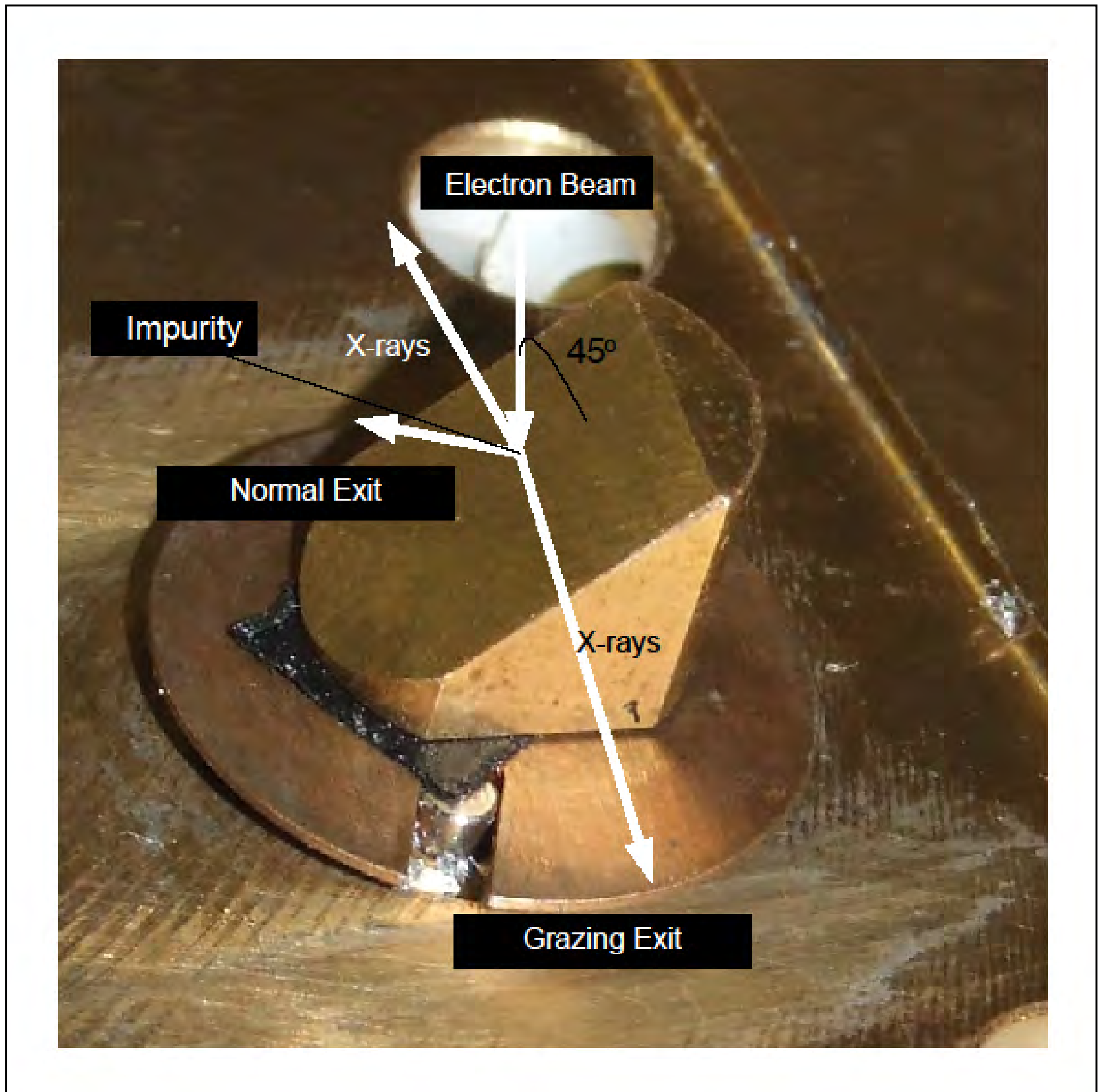

Fig 1 : A photo of the 45° inclined surface sample.

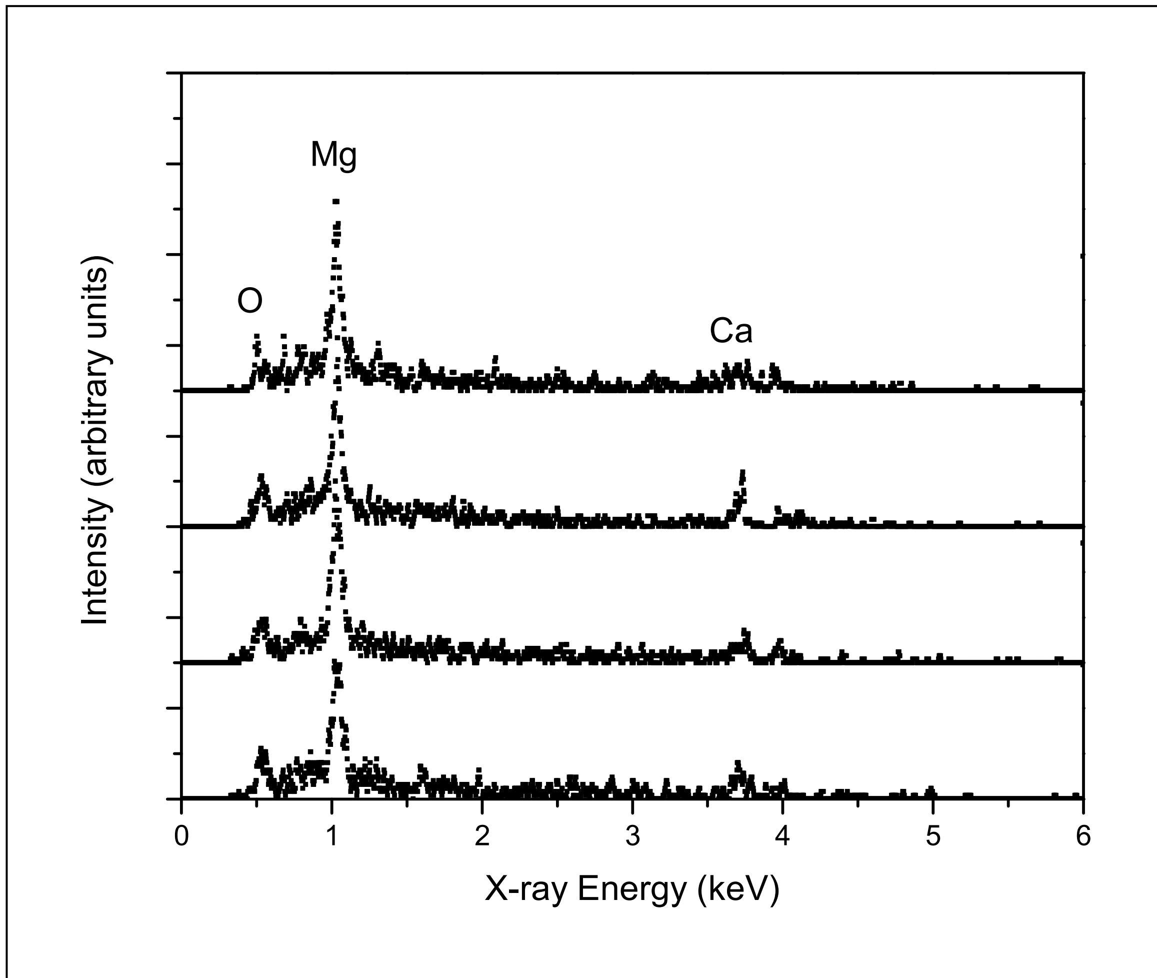

Fig 2: ED-XRF spectrum of the impurity on the 45° copper inclined surface.

Chapter 3 : Multilayer Nano-Thickness Measurement by a Portable Low-Power Bremsstrahlung X-ray Reflectometer

Abstract:

A low-power (1.5 W) portable Bremsstrahlung X-ray reflectometer (XRR) has been designed, realized and tested. The purpose of this apparatus is to measure thicknesses of multilayers within an X-ray beam energy range of 1-9.5 keV in industrial and research environments. Experiment has been carried out in this range with a measurement time of 10 min. The reflectometer apparatus was set up aligning the X-ray tube, sample holder and Si-PIN detector in one plane. A Mo/Si (9.98 nm) multilayer sample was used in the measurement. The direct beam intensity at (0.00^o) was measured. Intensity was measured at several glancing angles and reflectivity was calculated. Although one measurement is sufficient in a dispersive energy X-ray Reflectometer (XRR), measurement was taken at 0.45^o, 0.60^o and 0.80^o. The sample was tilted at an angle θ and the detector was linearly elevated corresponding to 2θ at each measurement. A calibration equation was proposed in equ. (1) to fit the apparatus geometry. Experimental reflectivity was calculated and compared to theoretical results. The portable X-ray reflectometer (XRR) was proved as feasible in multilayer nano-thickness measurement.

3.1 Introduction:

X-ray Reflectometry (XRR) has gained considerable interest during the last few decades. It is one of the non-destructive techniques used to assess multilayer structure properties [1-6]. It measures film thickness, interfacial roughness and density of films. It can be used to assess the physical properties of both single and multilayer structures [7-12].Two different techniques are mostly used in X-ray Reflectometry (XRR), namely, angle and energy dispersive methods [13].

In the angle dispersive method; a monochromatic X-ray beam is used and the angular scan is carried out either mechanically or by means of a spatially extended detector such as an image plate. In the energy dispersive method; XRR makes use of a polychromatic X-ray beam and scans the energy by means of an energy sensitive detector, making the fixed geometry during data collection an advantage over the angular dispersive method. A filter of a specific wavelength has to cover the X-ray detector Be window preventing it from damage or deteriorating by intense X-rays. However using the energy dispersive method involves dealing with problems of the simultaneous presence of photons having different energies, which interact in different ways with the sample material, it was verified that continuum X-rays from a low power X-ray tube can achieve a 1 ng detection limit by a portable TXRF spectrometer [14]. Utilization of many other X-ray characterization techniques has been adapted to many applications but there is still no available portable apparatus using XRR measuring the thickness of multilayers in the nano-scale range with a low power source. In this chapter we prove that nano-thickness measurement is possible using a low power continuum X-ray source by a portable X-ray reflectometer.

In this chapter we designed and developed a portable X-ray reflectometer. Continuum X-rays are used in the measurement. For continuum X-rays, the spectrum is measured as function of X-ray energy while it is measured as a function of glancing angle in case of monochromatic X-rays [15-19]. The power of the X-ray tube used is weak (1.5 watts) compared with previous works in related papers e.g. in synchrotron and rotating anode X-ray tube [20].

3.2 Experiment:

The principle used in this apparatus is the following: A tube of white X-rays irradiates the sample at glancing incidence. When X-rays hit the sample, they reflect off the sample surface. If the specimen is a thin film deposited on a substrate of a different composition, then the X-ray beam at grazing incidence will reflect off of both the film and substrate interfaces, producing an interference pattern that yields the thickness value of the thin film. A detector counts the reflected X-ray photons and measures their energies. The X-ray Reflectometry (XRR) spectrum is then recorded and analyzed. Fig.1 shows a) schematic view and b) a photograph of the portable X-ray reflectometer.

3.3 Apparatus description:

The design of the apparatus is not classical for an XRR instrument since it has an orthogonal geometry rather than a goniometric geometry, i.e. the X-ray tube, sample and detector are all in the same plane and the detector is moved linearly, not radially, unlike in a goniometer in the conventional apparatus. It is a portable apparatus, adaptable to a low-power X-ray source. In the apparatus we change the angle of the sample and the height of the detector according to the glancing angle at which the measurement is done. Although measurements for the different samples can be done at a fixed angle, changing the glancing angle and detector height is done to extra verify the results and make less error contribution to experiment. Low-power continuum X-ray source, adaptation to portability providing a portable set-up for X-ray reflectivity, straightforward and fast

measurement and lower cost make this apparatus easier to use and more available in laboratory to substitute higher cost apparatus. Continuum X-rays and much lower power make it applicable without a filter and not causing damage to the Be window.

The weight of the device, including the power supply amplifier, computer and other accessories, is less than 7 kg. The X-ray tube has a maximum voltage of 9.5 kV, a maximum current of 150 μA and a spot size of ~ 50 μm (V) x 10 mm(H) (Manufacturer HAMAMATSU PHOTONICS K.K., model L9491 with W Anode). The detector is an energy dispersive Si PIN detector.

3.4 Method description:

In a Si PIN detector; X-ray reflectivity of a multilayer is usually measured in a spectrometer as a function glancing angles by illuminating the sample with a specific wavelength. A monochromatic X-ray beam irradiates a sample at a grazing angle θ while the reflected intensity is recorded at a height corresponding to 2θ. 2θ is the angle from the Bragg-diffracted in the reciprocal space to the Bragg-reflected beam in the real space. In this chapter, X-ray reflectivity was measured as a function of energy at different angles. The X-ray tube; multilayer and detector are all on the same plane. The detector is aligned vertically. Since white radiation is used, the overall costs of energy-dispersive X-ray reflectivity measurement can be decreased by an order of magnitude. Measuring time was 600 s for each measurement. The X-ray tube power was 1.5 watts. The target in the X-ray tube was tungsten and the applied voltage was 9.5 kV less than that for

tungsten L_3 absorption edge energy (10.2 keV) so tungsten L line characteristic X-rays were not emitted from the X-ray tube. A collimator (50μm high; 10 mm wide; 12mm long) was placed between the X-ray tube and the Mo/Si multilayer. An energy dispersive Si PIN detector was used in the measurement [21-27].

A slit (150 μm) placed in front of the Si PIN detector window, served to cut off the angular and spectroscopic tails of the continuum X-ray beam incident on the mirror. A Mo/Si multilayer sample (50 layers, d =9.98 nm, dMo/d (Mo+Si) =0.4) deposited by magnetron sputtering was measured [29]. Elevating the sample, a white X-ray incident beam was fixed at a glancing angle θ. The reflected beam intensity was measured at an appropriate detector height corresponding to angle 2θ and reflectivity was calculated.

3.5 Results and discussion:

X-ray reflectivity (XRR) for the Mo/Si multilayer, inputting the same parameters provided by the manufacturer, was calculated using Berkeley Laboratory X-ray tools [28]. Reflectivity obtained by the portable X-ray apparatus was compared to calculated X-ray reflectivity. Reflectivity is obtained by dividing the intensity at a glancing angle by intensity at 0.00^o. Fig. 2 shows the data obtained by the apparatus at 0.00^o, 0.45^o, 0.60^o and 0.80^o as intensity versus X-ray energy. The spectrum at 0.00^o shows the intensity of the direct beam, it decays at 0.45^o and further decays at 0.60^o and 0.80^o. Fig.3 shows the experimental and the theoretical results of X-ray reflectivity as a function of X-ray energy at 0.45^o, 0.60^o and 0.80^o. The relative zero was taken at 0.02^o. Measurement angle can slightly differ from

theoretical angle by $\pm 0.02^{o}$. The decay of the total reflection as the glancing angle is getting further from 0.00^{o} is shown. The peak following is the first Bragg peak. Considering the experimental error and geometry of the apparatus, a calibration equation for reflectivity was obtained. Fitting with experimental results leads to a nonlinear response curve that can be fitted with good approximation with the following calibration equation:

$$R(reflectivity) = \frac{I}{I_0} \times \left(\frac{1}{\cos^2\theta} + \frac{A(\theta)}{\sin^2\theta} \right) \text{........(1)}$$

Where $\cos^2\theta$ and $\sin^2\theta$ are expressed in terms of intensity as follows:

$$\sin^2\theta = \frac{|I_0 - I|}{I}, \cos^2\theta = \frac{I}{I_0}$$

where I_0 stands for the incident intensity, I for the reflected intensity, θ for the glancing angle. A(θ) is an empirical value supposedly dependent on the angular deviation and slit diffraction , the experimental and theoretical curves are in good agreement when $A(0.45^{o}) = 0$, $A(0.60^{o}) = 1.2$ and $A(0.80^{o}) = 4$.

Though the thin film thickness is still concludable from the graphs without it; the calibration equation can make the experimental intensities in better agreement with the theoretical ones. Fig 4. shows the fitting of the calibration equation.

The sharp peak at around 3keV in the experimental spectrum is due to the Ar Kα peak. The experimental curves are less corresponding to the theoretical curves as the region of X-ray total reflection gets sharper. This can be to some extent due

to instrumental effects like imperfect collimation and the degree of inaccuracy. The Bragg peak in the theoretical and experimental spectra is more corresponding at 0.45^{o} than at 0.60^{o}, which in turn is more corresponding than at 0.80^{o}.

From Fig.3 thickness is directly obtained by the Bragg condition; e.g. the Bragg peak at 0.45^{o} (0.007rad) corresponds to 8.70 keV (0.14nm); applying the Bragg condition ($2d \sin\theta = n\lambda$), thickness will be 9.53 ± 0.45 nm. The Intensity difference calibrated in the suggested equation does not contribute to this value since thickness is deducted from the Bragg peak position. This slight difference and the difference in theoretical and experimental spectra in all the measurements were due to some problems concerning the accuracy of analysis. Any slight misalignment of the detector height could result in a less accurate detection angle of the reflected X-rays. As a result; reflectivity distribution might have changed and the X-ray flux might not be strong enough at 2θ. A shift of peaks with increasing angle might have been due to this reason. Another important source of error is that the X-rays reflected from the Mo/Si multilayer due to different glancing angles might not all have been precisely parallel because of X-ray divergence from the X-ray tube. This might have resulted in lower reflectivities at 0.60^{o} and 0.80^{o}. The intensity was very weak in the range below 2 keV because of the Be window. The mode of operation was a $\theta/2\theta$ mode (where θ is the glancing angle and 2θ is the detection angle) which assures the incident angle is always half of the angle of diffraction. The detector is heightened linearly with an instrument error of a micrometer. This can overall be a reasonable measurement since 1-10% variation of thickness and density happens after multilayer

fabrication due to surface effects. Bulk density is always assumed in the calculated curves.

Although the detection angle is moved linearly, the X-ray portable reflectometer (XRR) is adequate for detecting the reflecting beams due to small glancing angles and a calibration equation (1) to correct aberration has been proposed. Since polarization makes a negligible contribution at small angles, unpolarized beam was used. Since the reflection at the surface and interface is due to the different electron densities in the different layers, which correspond to different refractive indices, a manufacture error can always be present in a sample. The average density near the surface in a multilayer is less than the normal bulk value and presumably increases with depth. Oxidation can also occur during and after multilayer preparation.

Since the (Mo/Si) multilayer surface was glossy and white X-rays were used, specular reflection might not have been maintained and a combination of specular and diffuse reflection might have reflected off the multilayer surface.

3.6 Conclusion:

Despites its simple principle, the apparatus fulfills industrial needs in portable thin layer thickness measurement. Reference samples are needed for calibration; reference samples of known thickness are not needed. Further reduction of size and weight by highly integrated and miniaturized electronics can be done.

In this chapter we proved that continuum X-rays can be used for X-ray reflectivity measurement with a weak (1.5 watts) X-ray source. It provides the advantages of a continuum X-ray source in X-ray reflectivity; in terms of easiness of measurement; not associated with its usual problems related to strong intensity like sample damage, filter damage and provides less polychromatic effects. It also provides a portable apparatus for X-ray reflectivity. The portable apparatus presented is verified applicable in X-ray reflectivity measurement (XRR).

"X-ray reflectometry (XRR) is a nondestructive technique used to assess the multilayer structure properties, which measures the film thickness, interfacial roughness, and film density. No portable XRR instrument was available until a new portable XRR apparatus, which measures the thickness of multilayers on the nanoscale range, was developed. The reflectometer apparatus was set up by aligning the X-ray tube, sample holder, and Si-PIN detector in a single plane. The spectrum was measured as a function of the X-ray energy for the continuum X-rays used in the measurement, whereas the spectrum is measured as a function of the glancing angle for monochromatic X-rays. A Mo/Si (9.98 nm) multilayer sample was used to validate this instrument, and its feasibility for multilayer nanothickness measurements was confirmed."

(K. Tsuji, K. Nakano, Y. Takahasi, K. Hayashi and C. U. Ro, Anal. Chem., **84**(2012) 636–668.)

References:

1. L. G. Parratt, Phys. Rev. **95 (**1954**)** 359–369.
2. B. L. Henke, Phys. Rev. **A6 (**1972) 94–104.
3. D. K. G. de Boer， Phys. Rev. B4 (1991) 498-511.
4. A.D. Dane, A. Veldhuis, D.K.G. de Boer, A.J.G. Leenaers and L.M.C. Buydens, Physica. **B253** (1998) 254–268.
5. T. Salditt, D. Lott, T.H. Metzger, J. Peisl, G. Vignaud, J.F. Legrand, G. Gruebel, P. Hoghoi and O. Schaerpf , Physica. **B221**(1996) 13-17.
6. B.K. Tanner and J.M. Hudson, IEEE Trans. Magn. **28** (1992) 2736-2741.
7. J. Kawai, M. Takami, M. Fujinami, Y. Hashiguchi, S. Hayakawa, and Y. Gohshi, Spectrochim. Acta, **B47** (1992) 983-991.
8. K. Hayashi, H. Amano, T. Yamamoto, J. Kawai, Y. Kitajima, and H. Takenaka, Spectrochim. Acta, **B54** (1999) 223-226.
9. K. Hayashi, J. Kawai. Y. Moriyama, T. Horiuchi, and K. Matsushige, Spectrochim. Acta, **B54** (1999) 227-230.
10. K. Hayashi, S. Kawato, T. Horiuchi, K. Matsushige, Y. Kitajima, and J. Kawai, Appl. Phys. Lett. **68** (1996) 1921-1913.
11. J. Kawai, M. Sai, T. Sugimura, K. Hayashi, H. Takenaka, Y. Kitajima, X-Ray Spectrom. **28** (1999) 519-522.
12. P. Karimov, S. Harada, J. Kawai, Surf. Interface Anal. **35**, (2003) 76-79.
13. V.R. Albertini, B. Paci and A. Generosi, J. Phys. **D39** (2006) R461–R486.
14. S. Kunimura and J. Kawai, Anal. Chem. **79** (2007) 2593-2595.
15. A. Carapelle, K.Fleury-Frenette, J. Collette, H. Garnir and P. Harlet, Rev. Sci.

Instrum. **78** (2007) 123109-123111.

16. A. Attaelmanan, S. Larsson, A. Rindby, P. Voglis, and A. Kuczumow, Rev. Sci. Instrum. **65** (1994) 7-12.
17. C. Ribbing, M. Anderson, K. Hjort, and H. Lundqvist, Rev. Sci. Instrum. **74** (2003) 3423-3428.
18. A. Longoni, Nucl. Instrum. Methods. **A409** (1998) 407-409.
19. P. Dhez, H. Duval, J.C. Malaurent, J. X-ray Sci. Technol**. 3 (**1992) 176-193.
20. L. Kaihola, E.L.J.C. Malaurent, H. Duval and P. Dhez, J. Magn. Magn. Mater. **93** (1991) 176-93.
21. B. Lengeler, Adv.Mater. **2** (1990) 123-131.
22. J.C. Malaurent, H. Duval, J.P. Chauvineau, O. Hainaut, A. Raynal and P. Dhez, Opt. Commun. **173** (2000) 255-263.
23. T. C. Huang, R. Gilles, and G Will, Thin Solid Films. **230** (1993) 99- 101.
24. R. Felici, Rigaku J. **12(**1995) 11-17.
25. K. Orita, T. Morimura, T. Horiuchi and K. Matsushige, Synth. Met. **91**(1997) 155-158.
26. P. Karimov, S. Harada, H Takenaka and J. Kawai, Spectrochimia Acta. **B62** (2007) 476-480.
27. H. Takenaka, T. Kawamura and H. Kinoshita, Thin Solid Films. **288** (1996) 99-102.
28. Berkeley Lab. (http://henke.lbl.gov/optical_constants/multi2.html).

Figures:

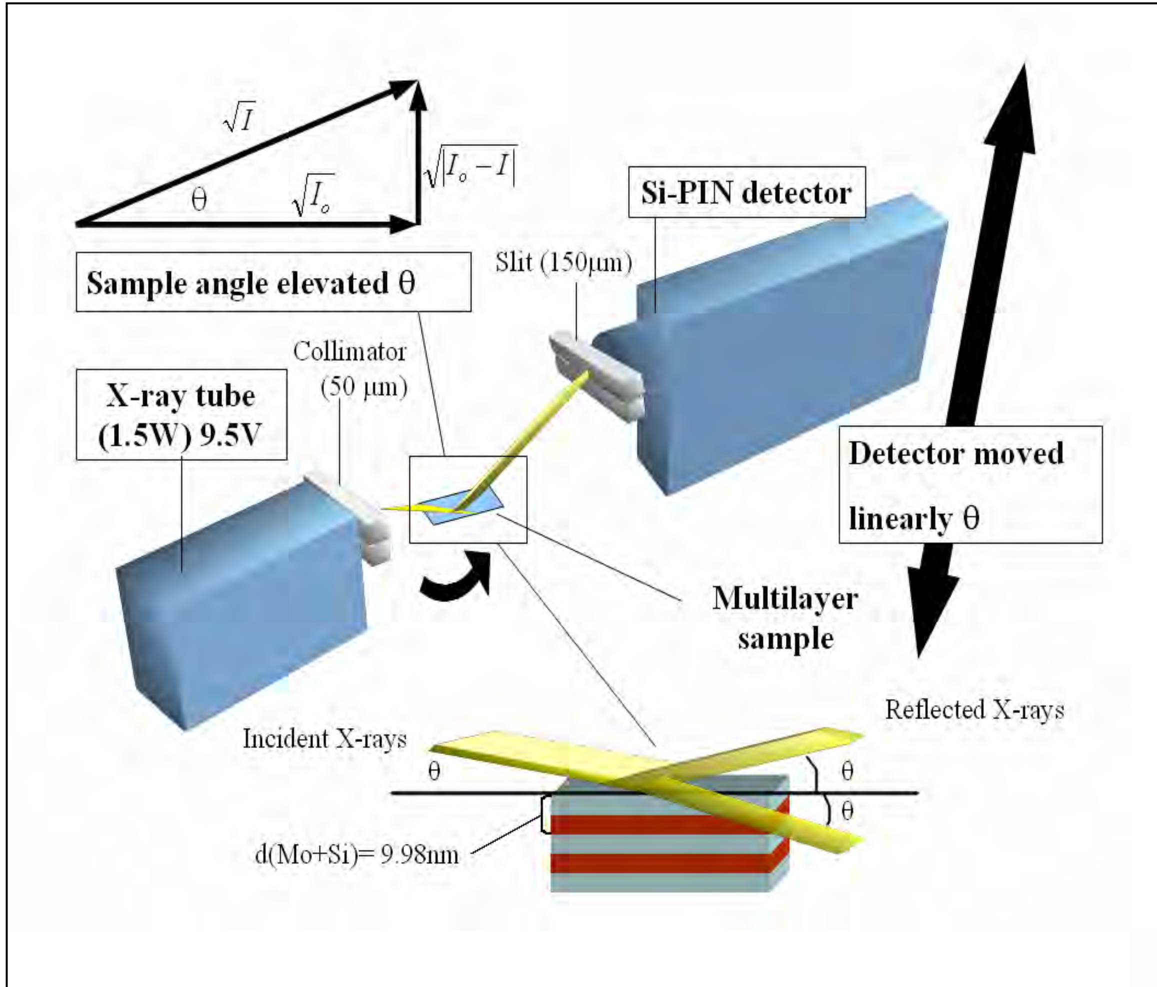

Fig 1: a) A schematic view of the portable X-ray reflectometer; fixed X-ray tube, sampled radially elevated θ and detector heightened at a position corresponding to 2θ .

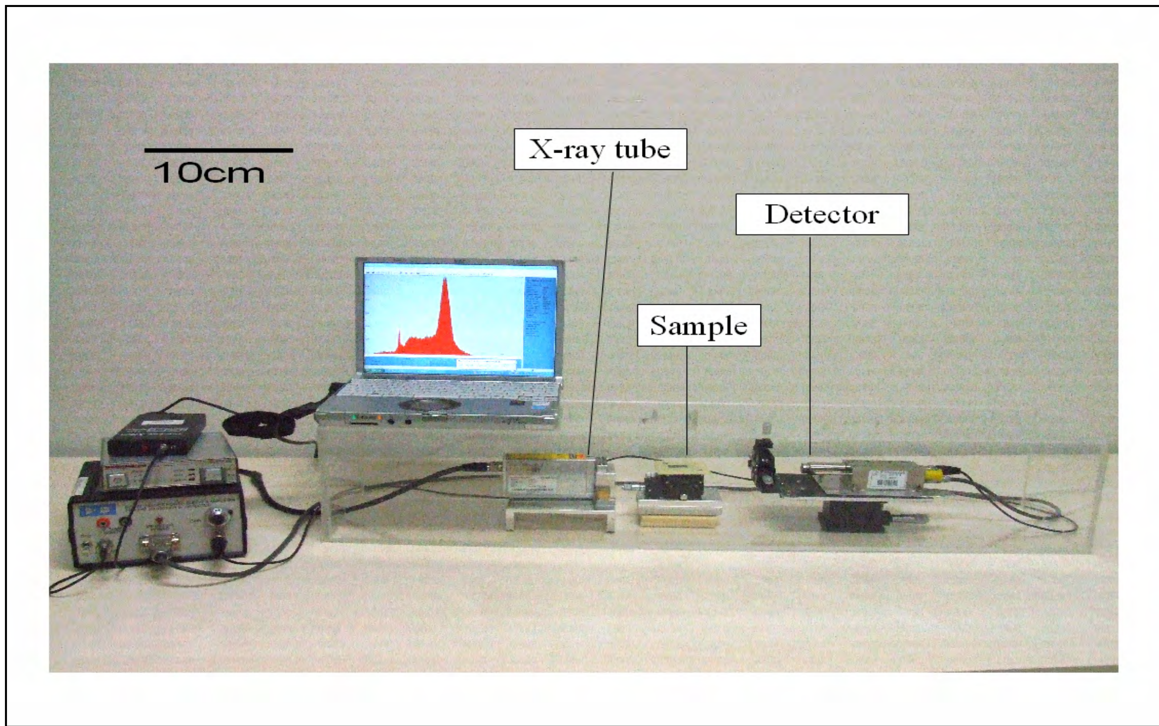

Fig 1: b) A photograph of the portable X-ray reflectometer.

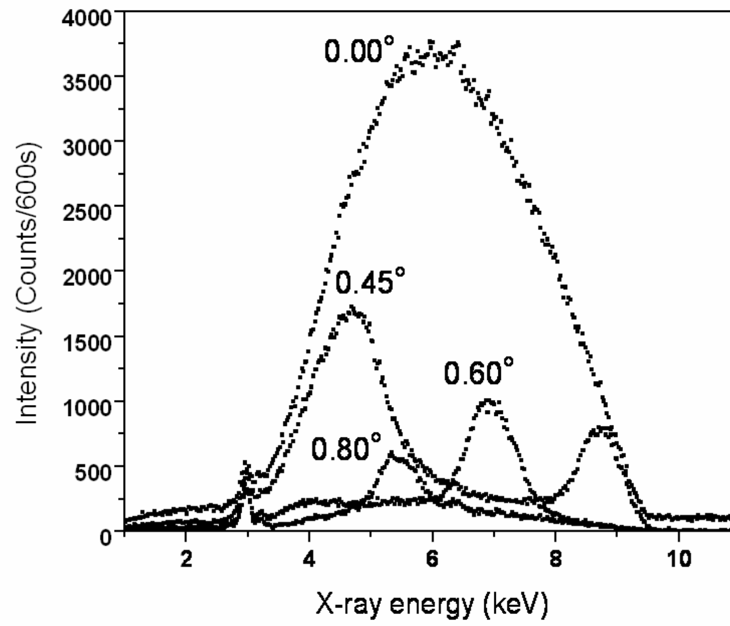

Fig 2: Intensity versus X-ray energy at (0.00°, 0.45°, 0.60°, 0.80°). Intensity at 0.00° is the direct beam.

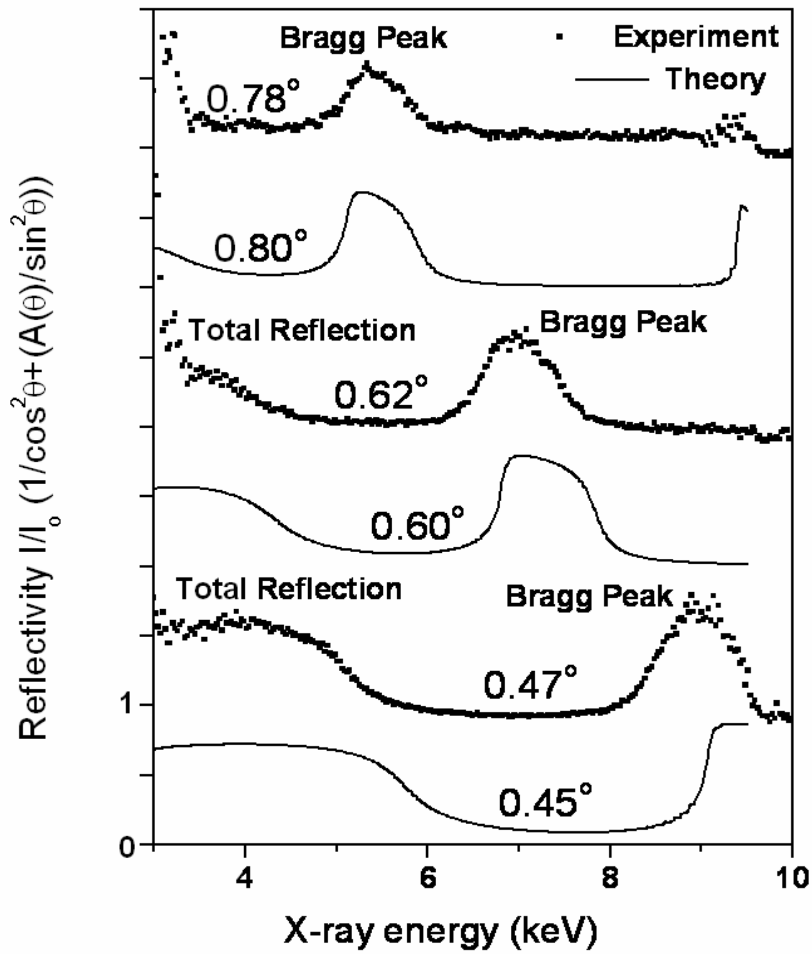

Fig 3: Reflectivity versus X-ray energy at (0.45°, 0.60°, 0.80°). The decay of the total reflection is followed by the first Bragg peak.

Fig 4: Reflectivity versus energy by the calibration equation at 0.60°.

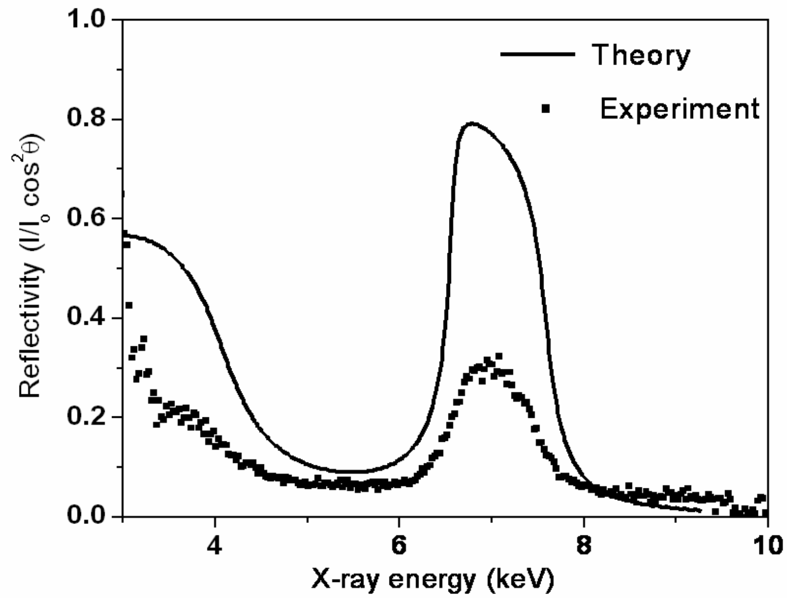

Fig 4: a) Measured Reflectivity of experimental X-ray Intensity versus X-ray energy compared with the net calculated reflectivity versus X-ray energy at 0.60°;

$$R(reflectivity) = \frac{I}{I_0} \times \left(\frac{1}{\cos^2 \theta} \right).$$

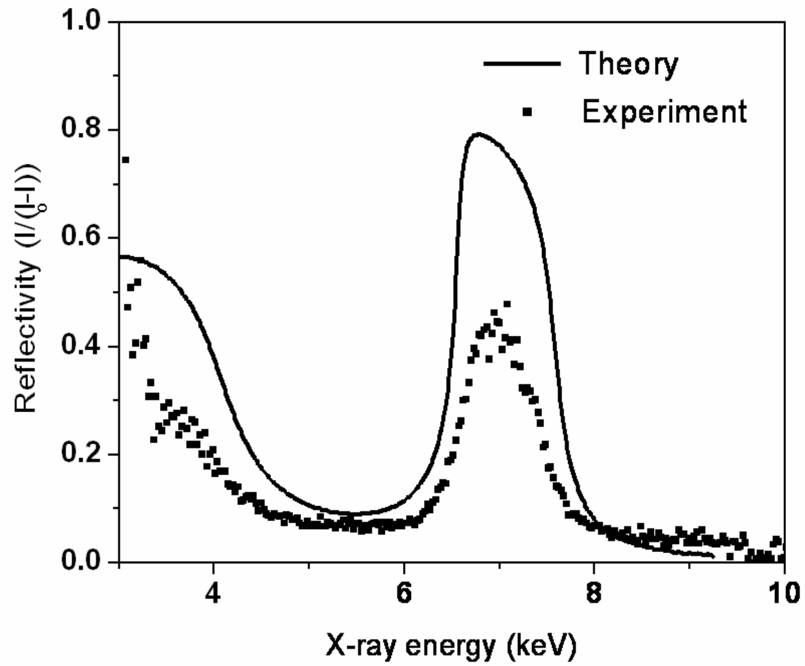

Fig 4: b) Measured Reflectivity of experimental X-ray intensity versus X-ray energy compared with the net calculated reflectivity versus X-ray energy at 0.60°;

$$R(reflectivity) = \frac{I}{I_0} \times \left(\frac{1}{\sin^2 \theta} \right).$$

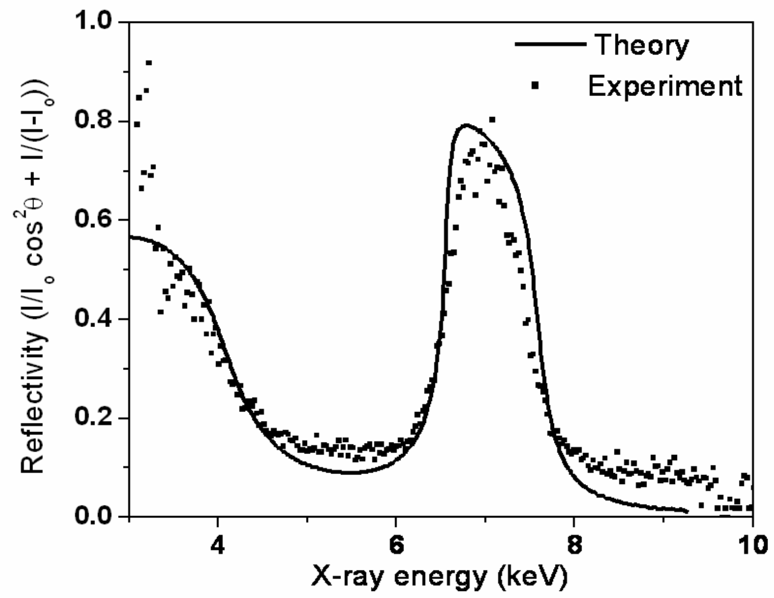

Fig 4: c) Measured Reflectivity of the sum of X-ray intensities versus X-ray energy compared with the net calculated reflectivity at 0.60^o;

$$R(reflectivity) = \frac{I}{I_0} \times \left(\frac{1}{\cos^2\theta} + \frac{1}{\sin^2\theta} \right) .$$

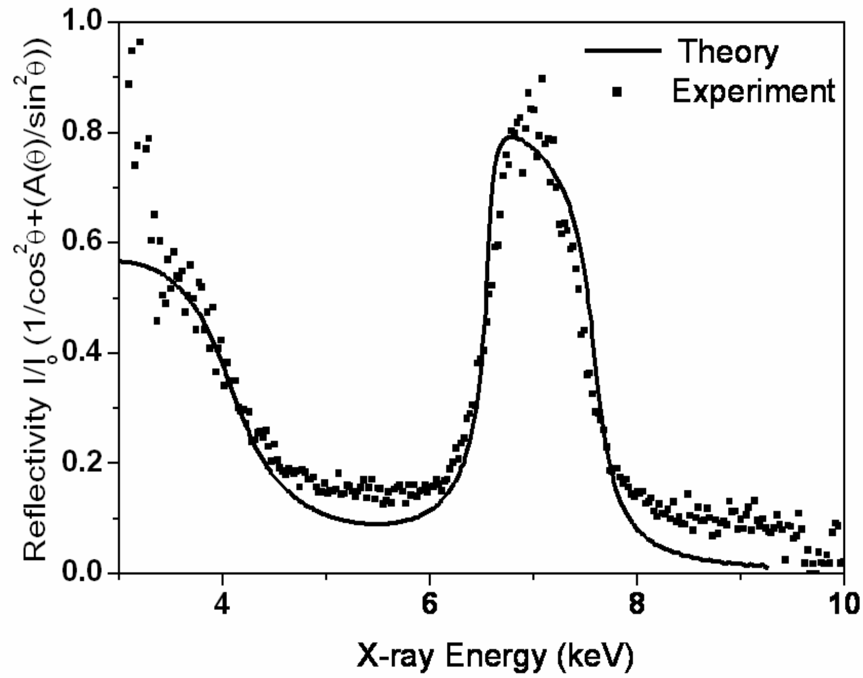

Fig 4: d) Measured Reflectivity of the sum of X-ray intensities, adding the radial constant, versus X-ray energy compared with the net calculated reflectivity at 0.60^{o}; $R(reflectivity) = \frac{I}{I_0} \times \left(\frac{1}{\cos^2 \theta} + \frac{A(\theta)}{\sin^2 \theta} \right)$.

Chapter 4: Analysis of a Hard Disk Top- Layer by Total Reflection X-ray Photoelectron Spectroscopy (TRXPS)

Abstract:

Photoelectron spectra from a typical hard disk storage media were measured at total reflection and non-total reflection conditions by changing the X-ray grazing angle by 0.1^{o} steps. The chemical analysis resulted in F, O, N and C usually making the upper layer of a typical hard disk medium. We observed enhancement of photoelectron emission of the top layer at total reflection. Pt and Co were only found by non-total XPS because they are constituents of a deeper region than the top and interface region. TRXPS is demonstrated to be characterizing hard disk upper layers.

4.1 Introduction:

Total reflection X-ray photoelectron spectroscopy (TRXPS) is usually performed by measuring photoelectron intensity at grazing incidence. It is ideally suited to providing critical information on elemental analysis, chemical state and depth. However, it is little used in industrial applications. Kawai authored a review of TRXPS including most applications till 2010 [1]. Since it was proposed by Henke [2], it has been used in many applications. Mehta and Fadley [3, 4] applied the method to investigate the surface chemical state of Si wafers and carbon containing over layers on Au. Kawai et al. [5, 6] proved that TRXPS reduces the inelastic background because of the limited penetration of the X-rays. The method has been proved useful in characterizing different types of multilayers [7, 9] and CMOS gate dielectrics [10-15]. In this chapter, we demonstrate TRXPS as applicable in hard disk top layer analysis. Because X-rays penetrate deeper than 2

nm in conventional XPS, TRXPS is proposed to mainly characterize the top layer [16-18].

4.2 Experiment:

TRXPS measurements were performed with a JEOL TRXPS Spectrometer, JPS 9010 TRX, using monochromatized Al $K\alpha$ (hν= 1486.6 eV) radiation with a quartz monochromator. The X-ray beam size was restricted to 5 mm $\times$ 10 mm. The pass energy was 50 eV for the wide scan measurement, 30 eV for the narrow scan and the base pressure of the vacuum chamber was 10^{-6} Pa. The spectra were obtained with an electron spectrometer consisting of a concentric hemispherical analyzer with a 10 cm long central orbital radius and a multi- micro-channel plate type detector. The spectrometer was calibrated by the Au 4f photoelectron peak. The X-ray tube input was 12 kV and 30 mA and the intensity counting rate of the spectrometer was 13500 cps with 5 channels per second. The sample was tilted manually. Wide scan measurements were carried out at 1.5^o, 4.0^o and 10.0^o glancing angles. The time to measure one spectrum was typically 10 minutes. No further processing such as lubrication or burnishing of the disk was performed prior to the XPS investigation. No electron charging was observed during measurement. Fig.1 shows a schematic illustration of the experimental set-up of TRXPS.

4.3 Results and discussion:

XPS wide-scan spectra of a typical disk at total reflection 1.5^{o} and at non-total reflection, 4.0^{o} and 10.0^{o}, are shown in Fig.2. It exhibits a series of intense sharp peaks arising from the direct excitation of electrons from core levels. Prominent among them are the for C, O and F 1s peaks. In addition to X-ray photoelectrons emitted from the surface, X-ray induced Auger (KLL) peaks C, O, and F are also seen. Considering a typical hard disk; C, N, F, Co, Pt are observable. Apart from appearance of Pt, N and Co peaks, C is assigned for the diamond-like carbon (DLC) and the prominent O is assigned for contributions from the top and the magnetic layers. Mainly the top surface elements; C, N, O, F are observable at 1.5^{o}. The TRXPS survey indicates the uppermost layer contains contributions from hydrocarbon because the C peak does not change with angle; with the spectra showing a C 1s peak at 285.0 eV as well as a well resolved peak at 293.3 eV that stands for the C-F bond [20]. N 1s, usually making the interface of the top and the lower magnetic layer, was also observable with slightly more photoelectron yield in TRXPS than in ordinary XPS. F 2s was only seen in TRXPS. The XPS wide scan at 4.0^{o} yielded less background than at 10.0^{o} with exactly the same elements except a more prominent Co 2p at 4.0^{o}. The least background and best sensitivity was obtained at 1.1^{o} which mainly detected the top-layer elements. Fig.3 shows the measured narrow scan 1s spectra of a typical hard disk at several angles for C, N, O and F. The delicate nature of the C-F bond over-layer is demonstrated by the C 1s spectra in Fig.3. The peaks 293.3 eV and

285.0 eV assigned to the C-F bond layer and C-C respectively [22]. The C-F intensity 293.3 eV increased at the region of total reflection.

The spectra were taken over a range of incident angles from 0.5^o to 4.0^o in 0.1^o steps and at 10.0^o. The angular deviation is attributed to the surface roughness since the top layer is not ideally smooth because it tends to pile up rather than to spread all over the surface as explained by *Wood* in [19], and because of the combination of layers due to the top layer material bonded to the diamond-like carbon surface.

Fig. 4 shows the normalized to F 1s grazing angle dependency of the narrow scan photoelectron intensity in a typical hard disk. The critical angle was found to be 1.1^o with δ is 1.82×10^{-4} with an electron density of 5.93×10^{23} electrons/cm^3 [14]. With δ stands for the difference from 1 of the refractive index, i.e., $n=\delta-1$.

The critical angle at all narrow scans was 1.1^o for all the elements. The peak 689.7 eV in Fig.3 is attributed to C-F bond usually used in hard disk top layer [22].

This chapter reports for the first time a TRXPS measurement of a hard disk top layer. Due to its shallow penetration, it mainly exhibited peaks of elements constituting the top layer.

4.5 Conclusion:

In summary, we have carried out TRXPS measurements on a typical hard disk and compared them to non-total reflection XPS. The background due to inelastic scattering of photoelectrons is reduced to one half in case of TRXPS as compared

to non-total XPS. At TRXPS (1.5^o), mainly the top layer elements; C, N, O, F are observable with more sensitivity and stronger intensity, which shows the C-F bond chemical shift as a surface protection layer.

References:

1. J. Kawai, J. Electron Spectrosc. Relat. Phenom. **268** (2010) 178-272.
2. B. L. Henke, Phys. Rev. **A6** (1972) 94-104.
3. M. Mehta and C.S. Fadley, Phys. Lett. **55A** (1975) 59-61.
4. M. Mehta and C.S. Fadley, Chem. Phys. Lett. 4**6** (1977) 225-230.
5. M. J. Chester and T. Jach, Phys. Rev. **B48** (1993) 17262-17270.
6. K. Hayashi, S. Kawato, T. Horiuchi, K. Matsushige, Y. Kitajima, H. Takenaka, and J. Kawai, Appl. Phys. Lett. **68** (1996) 1921-1923.
7. J. Kawai, H. Amano, K. Hayashi, T. Horiuchi, K. Matsushige, and Y. Kitajima, Spectrochim. Acta, Part **B 52** (1997) 873-879.
8. M. J. Chester and T. Jach, J. Vac. Sci. Technol. **B 11** (1993) 1609-1613.
9. S. Mickevičius, S. Grebinskij, V. Bondarenka, H. Tvardauskas, B. Vengalis, K. Šliužienė, B.A. Orlowski and W. Drube, Opt. Appl. **36** (2006) 235- 243.
10. M. J. Chester and T. Jach, and S. M. Thurgate, Nucl. Instrum. Methods **347A** (1994) 507-509.
11. J. Kawai, S. Kawato, K. Hayashi, T. Horiuchi, K. Matsushige, and Y. Kitajima, App. Phys. Lett. **67** (1995) 3889-3891.
12. M. J. Chester and T. Jach, and S. M. Thurgate, Rev. Sci. Instrum. 65 (1994) 339-342.
13. T. Jach, J. Gormley, and S. Thurgate, Spectrochim. Acta, Part **B 54** (1999) 1539-1544.

14. J. Kawai, M .Takami, M. Fujinami, Y. Hashiguchi, S. Hayakawa, and Y. Gohshi, Spectrochim. Acta, Part **B 47** (1992) 983-991.
15. J. Kawai, S. Hayakawa, Y. Kitajima, K. Maeda, and Y. Gohshi, Total reflection X-ray photoelectron spectroscopy, J. Electron Spectrosc. Relat. Phenom. 76 (1995) 313-318 .
16. L.G. Jacobsohn, D.F. Franceschini,M.E.H. Maia da Costa, and F.L. Freire Jr., J. Vac. Sci. Technol. 18A (2000) 2230-2238 .
17. T. E. Karis, G. W. Tyndall, D. Fenzel-Alexander, and M. S. Crowder, J. Vac. Sci. Technol. 15A (1997) 2382- 2387.
18. C. Donnet, J. Fontaine, A. Grill, V. Patel, C. Jahnes, and M. Belin, Surf. Coat. Technol. 94 (1997) 531-536.
19. R. Wood, IEEE Trans. Magn. 36 (2000) 36-42.
20. D. T. Clark, W. J. Flast, P. J. Tweedole, and H. R. Thomas, ESCA applied to polymers. XXVI. J. Polym. Sci., Polym. Chem. Ed. 18 (1980) 1651-1664.
21. Gangal, S. V., “Polytetrafluoroethylene, Homopolymers of Tetrafluoroethylene,” in Encyclopedia of Polymer Science and Engineering, 2nd ed., John Wiley & Sons, New York 1989.
22. G.Beasmon and D. Briggs, High Resolution XPS of Organic Polymers, The Scienta ESCA300 Database, first ed., John Wiley & Sons, London 1992.

Figures:

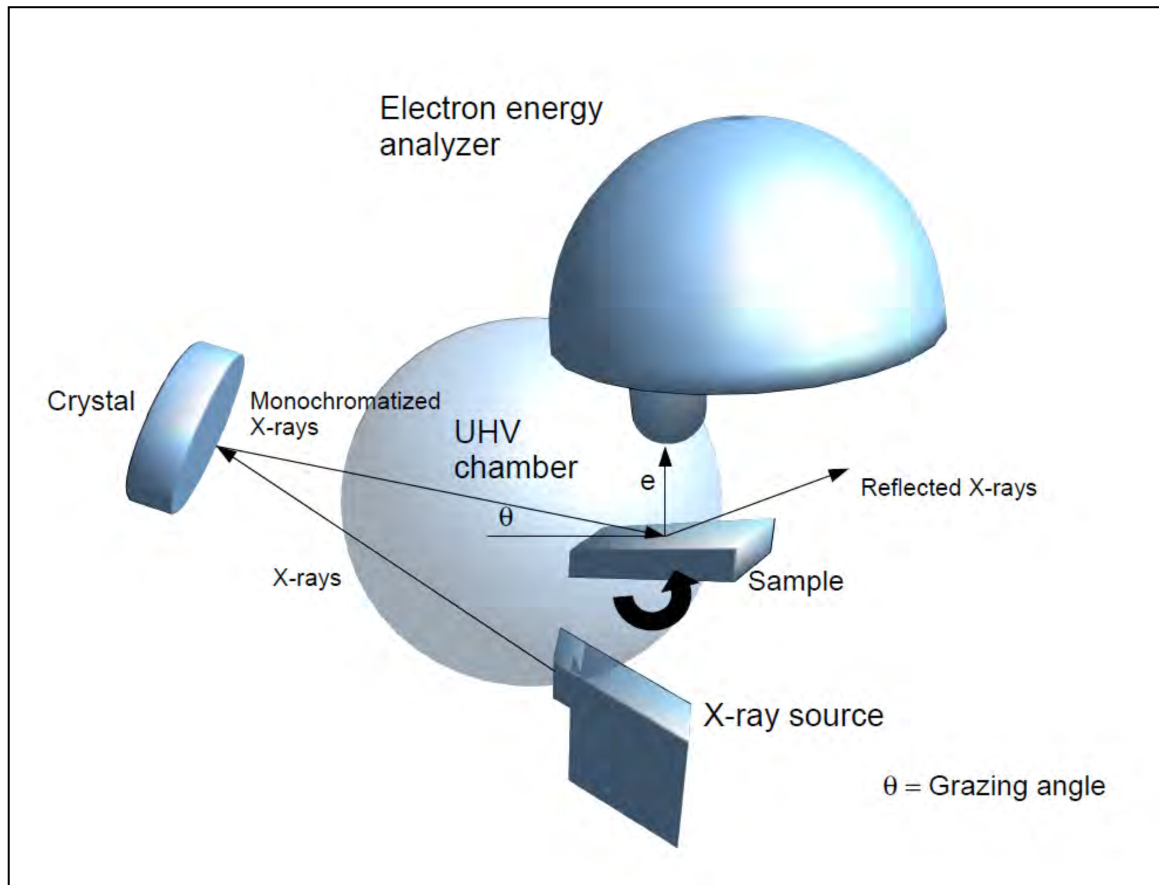

Fig 1: A schematic illustration of the experimental set up of TRXPS.

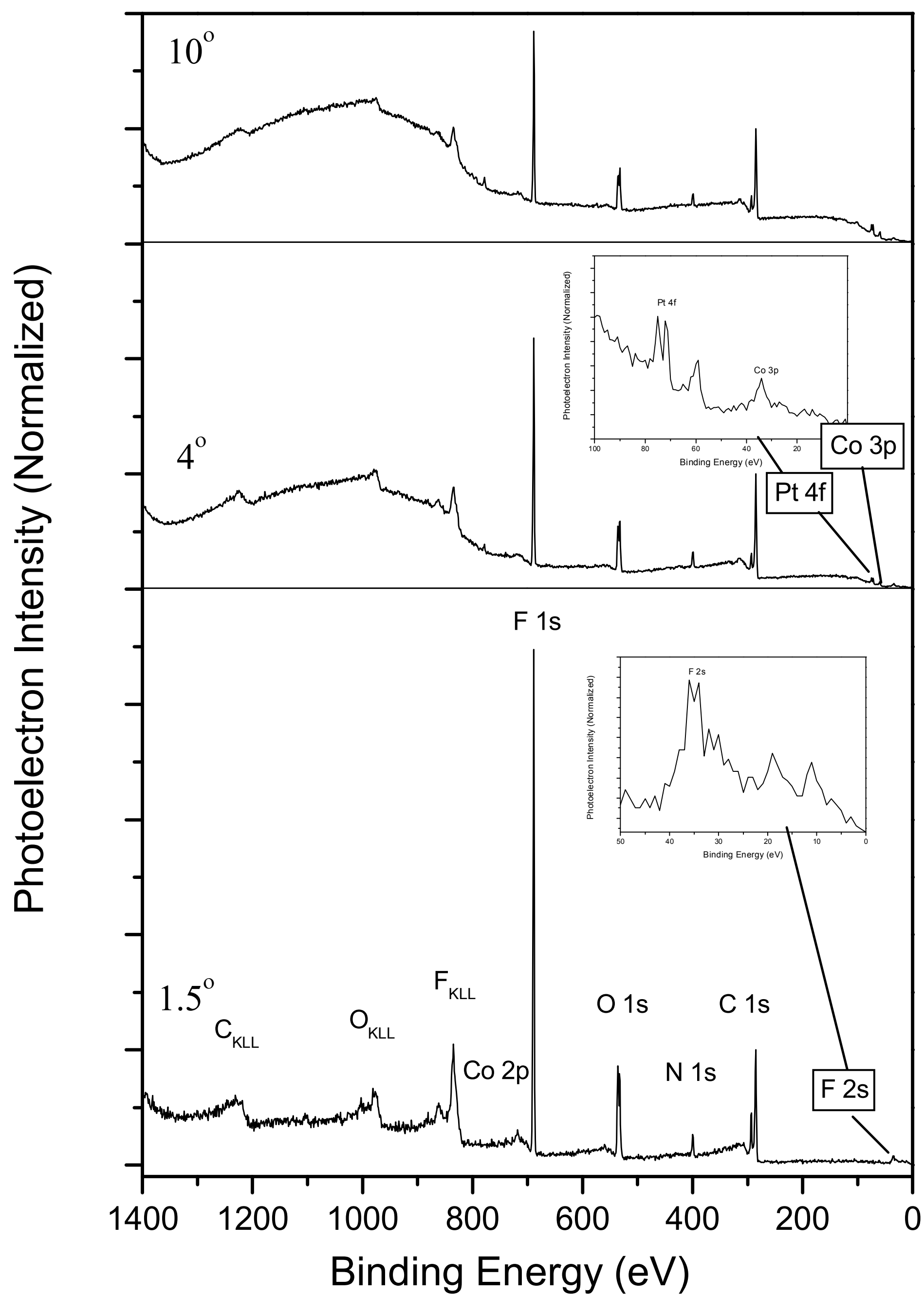

Fig 2: XPS wide scan of a typical hard disk media at total reflection (1.5^o) and non-total reflection (4°, 10°); normalized to C 1s.

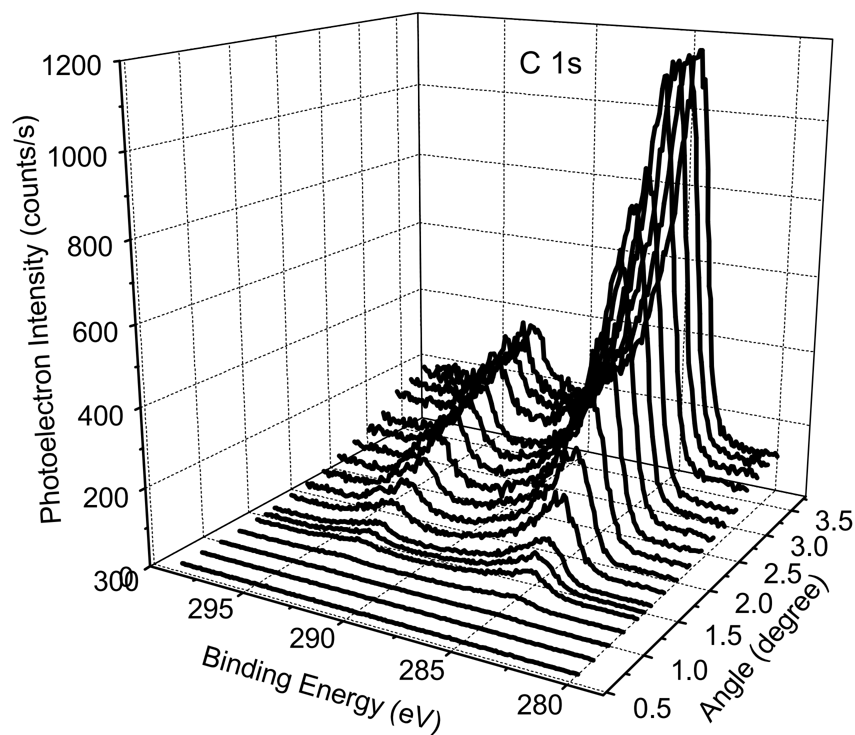

Fig 3: a) Raw data narrow scan of a typical hard disk media at C 1s (293.3 eV binding energy) at several angles.

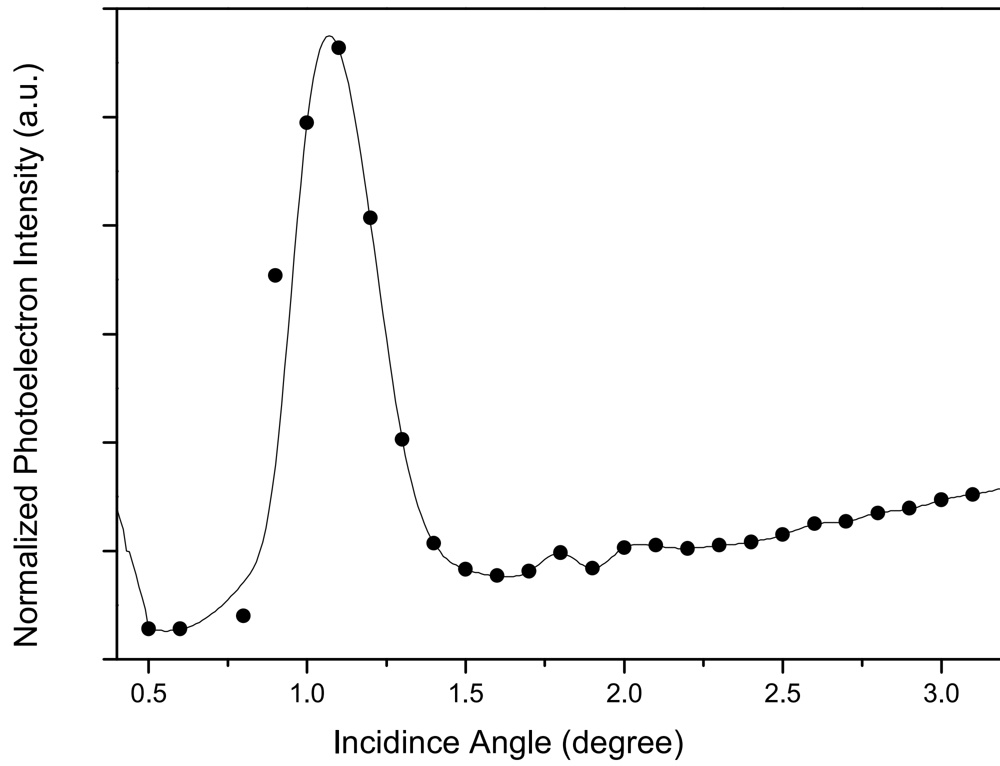

Fig 3: b) Normalized to C 1s- grazing angle dependency of C-F (293.3 eV binding energy) photoelectron intensity in a typical hard disk media.

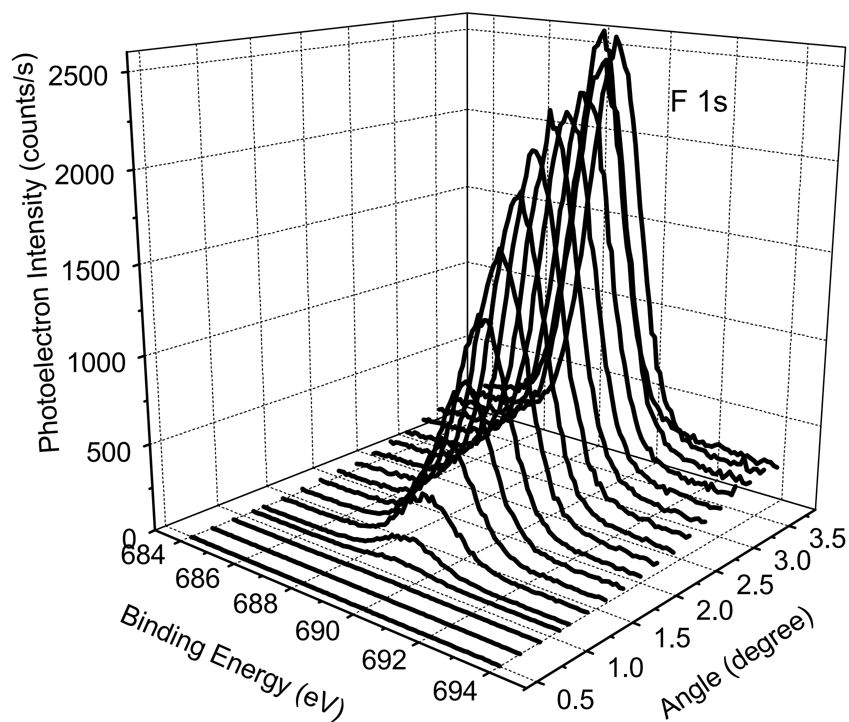

Fig 4: a) Raw data narrow scan of a typical hard disk media at C 1s (689.1 eV binding energy) at several angles.

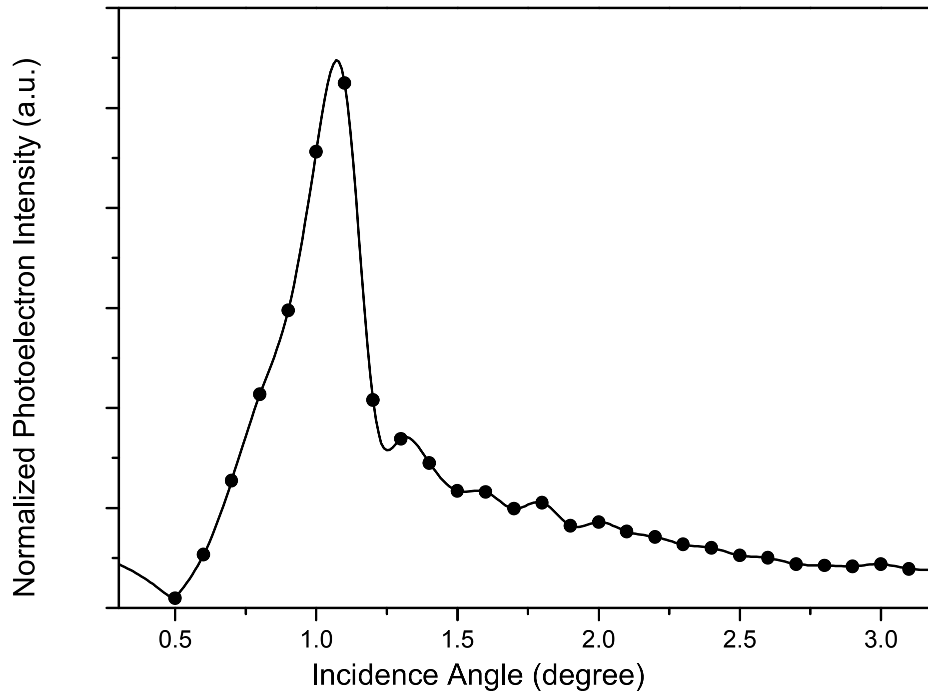

Fig 4: b) Normalized to C1s- grazing angle dependency of F 1s (689.1 eV binding energy) photoelectron intensity in a typical hard disk media.

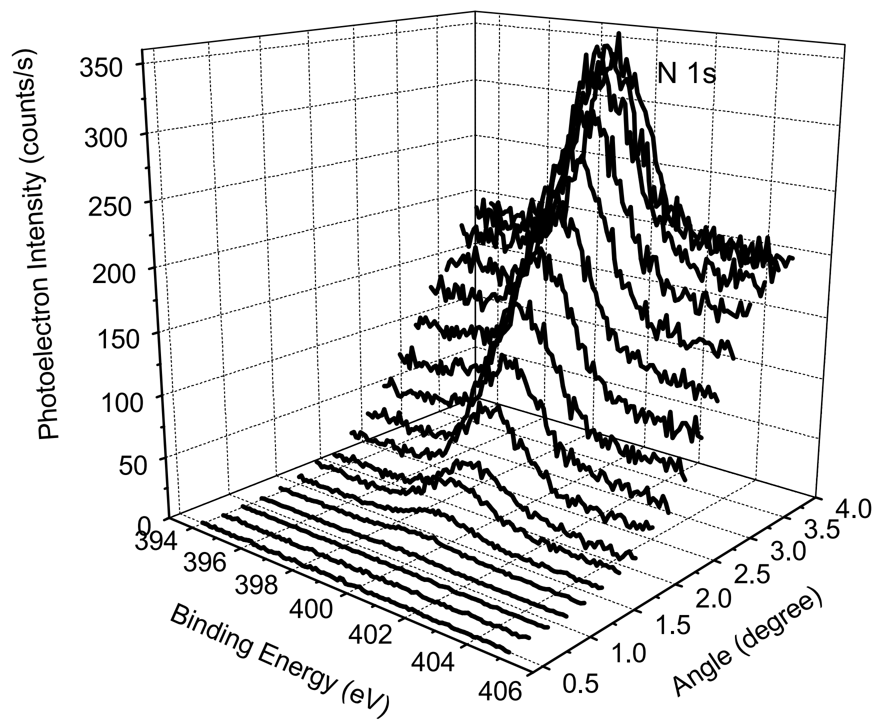

Fig 5: a) Raw data Narrow scan of a typical hard disk media at N 1s (399.5 eV binding energy) at several angles.

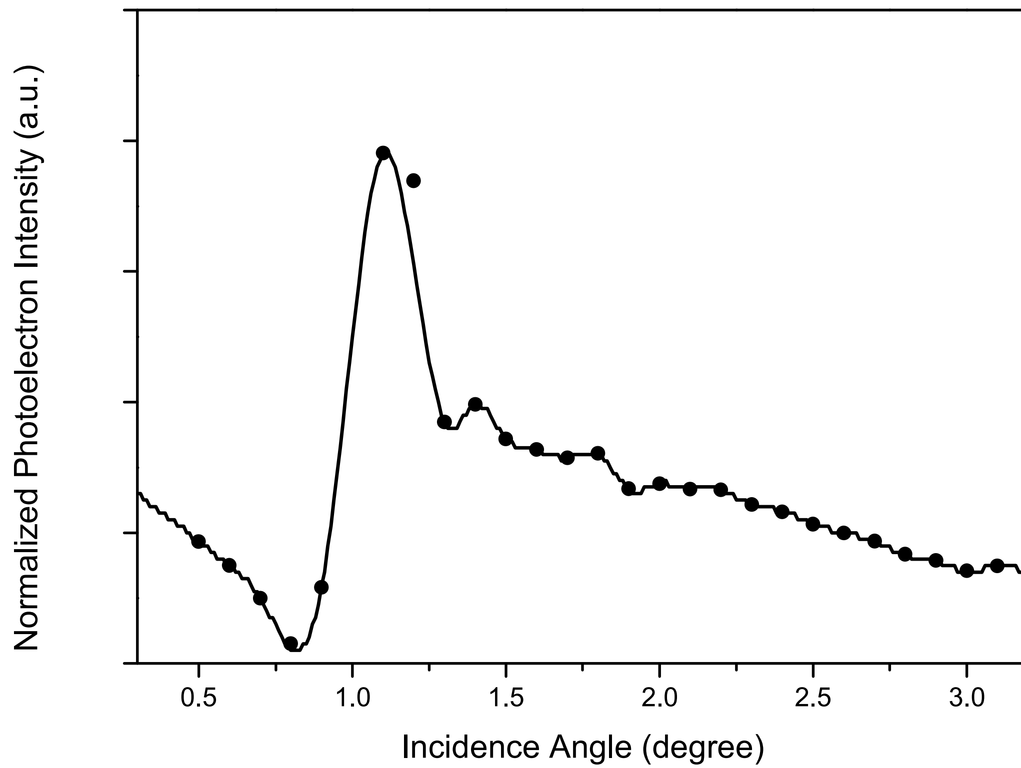

Fig 5: b) Normalized to C 1s- grazing angle dependency of N 1s (399.5 eV binding energy) photoelectron intensity in a typical hard disk media.

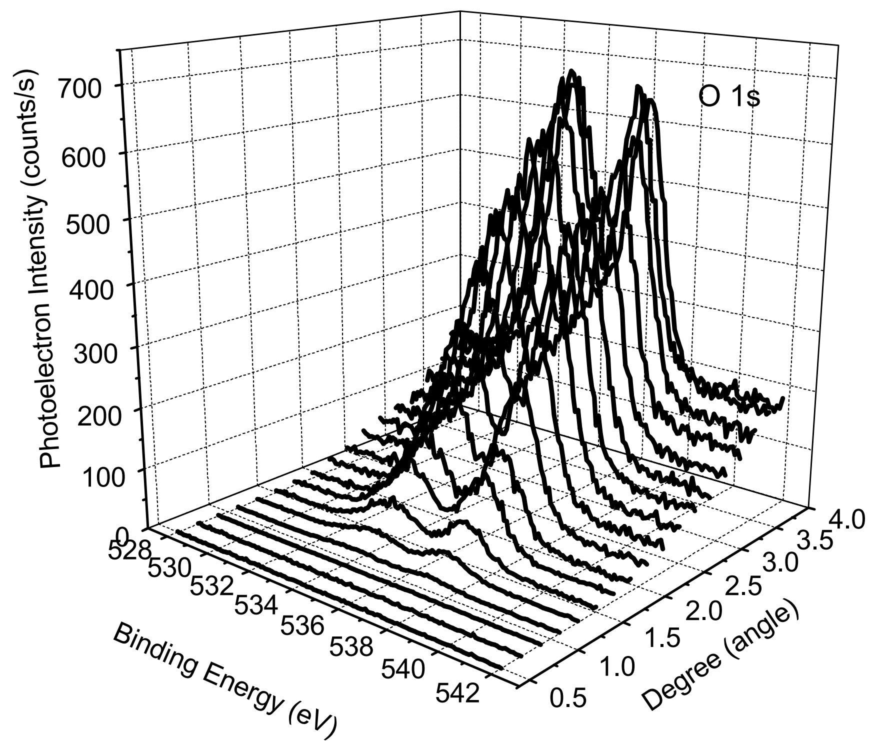

Fig 6: a) Raw data narrow scan of a typical hard disk media at O 1s (532.5 eV and 535.8 eV binding energies) at several angles.

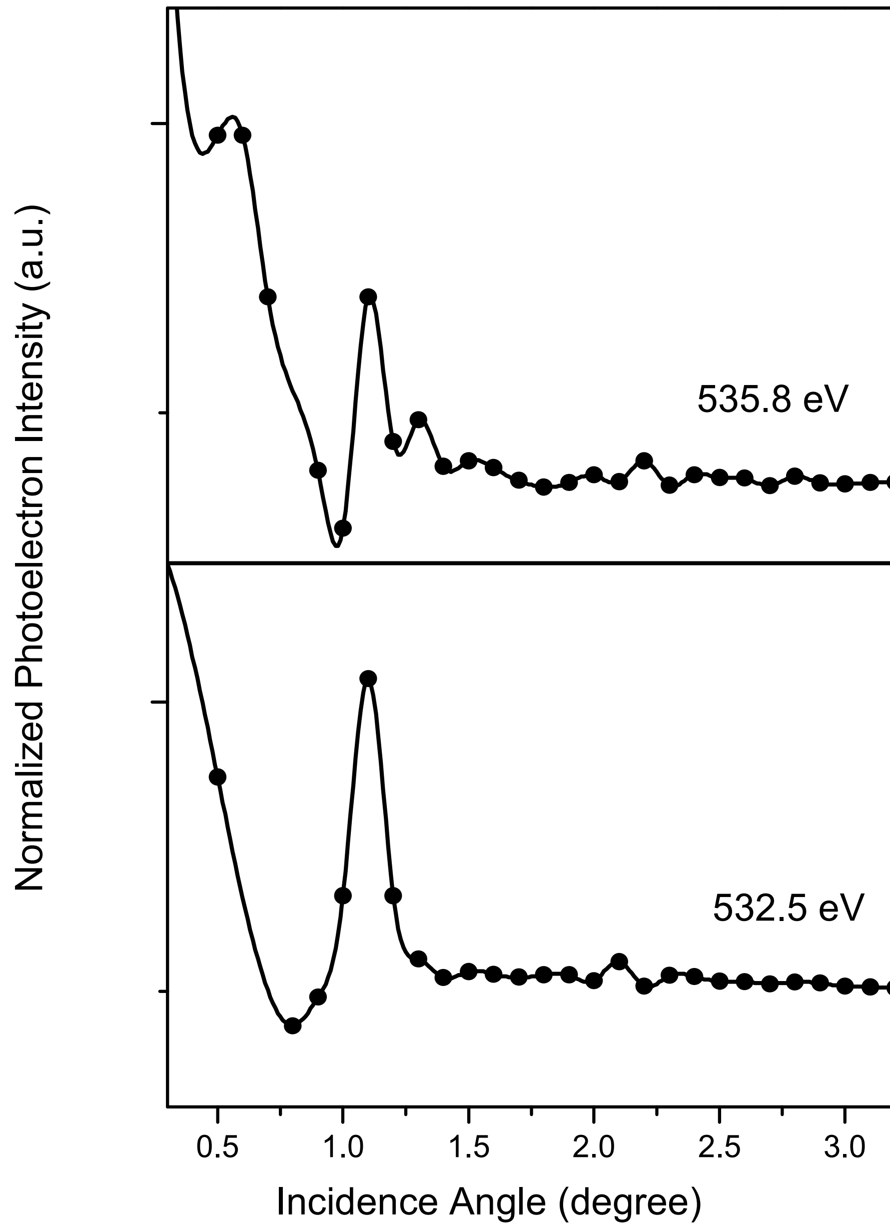

Fig 6: d) Normalized to C1s- grazing angle dependency of O 1s (532.5 eV and 535.8 eV binding energies) photoelectron intensity in a typical hard disk media.

Chapter 5: Hard Disk Top Layer Analysis by Total Reflection X-ray Photoelectron Spectroscopy (TRXPS): Effect of Acetone Rinsing.

Abstract:

We measured photoelectron spectra from a typical hard disk storage media at total reflection and non-total reflection at unburnished and acetone-cleaned conditions. F, O, N and C usually making the upper layer of a typical hard disk medium were detected. We observed enhancement of photoelectron emission of the top layer at total reflection. Pt and Co were only found by non-total XPS because they are constituents of a deeper region than the top and interface region. Ultrasonic acetone-cleaned and non-acetone-cleaned top layers were compared at total and non-total reflection conditions. TRXPS is demonstrated to be a powerful tool for storage media lubrication layer chemical state analysis, reproducible and reliable.

5.1 Introduction:

Total reflection X-ray photoelectron spectroscopy (TRXPS) combines aspects of both X-ray reflectivity and conventional X-ray photoemission spectroscopy (XPS) [1, 2]. In this method, a series of photoelectron spectra are obtained over a range of incidence angles in the vicinity of total reflection. The respective heights of peaks in the spectra are consequences of X-ray fields occurring from Fresnel conditions set up at the boundaries of the layer near the surface. The advantage of this method is the incorporation of the optical constants of the layers, as well as the photoelectron emission cross-sections of the elements and the mean free paths of the escaping photoelectrons, to fit the non-linear variation of the photoemission spectra as a function of the incidence angle. Although total reflection X-ray photoelectron spectroscopy (TRXPS) is ideally suited to providing critical

information on elemental analysis, chemical state and depth, it is little used in a quality control environment [3]. Since it was proposed by Henke [4], few experimental results have been reported. The first observation of surface atom XPS enhancement was by Mehta and Fadley using the method to investigate the surface chemical state of Si wafers and carbon containing over layers on Au [5]. Kawai et al. proved TRXPS reduces the inelastic background because of the limited penetration of the X-rays [6, 7]. The method has proved useful in characterizing different types of multilayers [8, 10] and CMOS gate dielectrics [11-17]. Abbas et al. demonstrated TRXPS as applicable in hard disk industry [2]. Using TRXPS, they demonstrated the chemical elemental characterization of computer hard disk media (Western Digital Model: WDAC33100-76H) top layer. Beside the small incidence angles in TRXPS, results for XPS are not always very reproducible due to problems with e.g. contamination and degradation. Chemical and morphological heterogeneity is known to affect reliability and reproducibility of any surface method. In the case of low Z thin films, this issue is challenging enough. In the case of XPS on fluorocarbon thin films, issues related to sample contamination and stability make evaluation more complicated [17-21]. Stability issues for organic materials and polymers during XPS experiments are also important for reliable data; X-ray induced irradiation damage, adsorption or desorption of volatile species in ultra high vacuum may distort the data considerably. In addition, sample charging and small angle tilting may further complicate the data interpretation.

In this chapter, we produce the same data from a different hard disk sample (Hitachi Model: HTS541660J9AT00) demonstrating the hard disk media top layer by TRXPS is reproducible for other hard disk media.

5.2 Experiment:

TRXPS measurements were performed with a commercially available (JEOL TRXPS Spectrometer JPS 9010 TRX) using monochromatized Al-$K\alpha$ (hν= 1486.6 eV) radiation with a SiO_2 $(10\bar{1}0)$ (2d =0.6686 nm) monochromator. The X-ray beam size was restricted to 5 mm$\times$10 mm. The pass energy was 50 eV for the wide scan measurement, 30 eV for the narrow scan and the base pressure of the vacuum chamber was 10^{-6} Pa. The spectra were obtained with an electron spectrometer consisting of a concentric hemispherical micro-channel plate type analyzer with a 10 cm long central orbital radius. The spectrometer was calibrated by reference to the Au *4f* photoelectron peak. The X-ray tube input was 12 kV and 30 mA and the intensity counting rate of the spectrometer was 13500 cps with 5 channels per second. The sample was tilted manually. Measurements were carried out at 1.5^{o}and 10.0^{o} to the surface for acetone and non-burnished surfaces. The acetone cleaned hard disk top surface was also exposed to 120 minute ultrasonic before measurement.

5.3 Results and discussions:

XPS wide-scan spectra of a typical disk media at total reflection 1.5^o and at non-total reflection, 10.0^o, for both the burnished and non-burnished conditions are shown in Fig.1. It shows a series photoelectron intensity peaks. Prominent among them are the C 1s, O 1s and F 1s. Auger peaks [F (KLL), O (KLL), and C (KLL)] are also seen. Since they are main elements in a typical hard disk media; F, C, Co, Pt, N are observable. Apart with Pt, N and Co peaks, C and O are attributed to the contribution from ambient. At TRXPS (1.5^o), only the top surface elements; F, C, O, N are observable. With the relative zero at ± 0.4 eV, the TRXPS wide scan shows the top lubrication layer is composed of hydrocarbon (probably environmental contamination); with the spectra showing a C 1s peak at 285.0 eV (binding energy) as well as the fluorocarbon over-layer, with a peak at 293.3 eV (20). O 1s implies that the surface of the fluorocarbon also contains adsorbed oxygen. N 1s, usually making the interface between the lubrication layer and deeper ones, is also observable with slightly more photoelectron yield in TRXPS than in ordinary XPS. F 2s is only seen in TRXPS. Although the intensity of fluorine had a small decrease after cleaning, the chemical analysis was the same in both and after cleaning. The least background and best sensitivity was obtained at total reflection at 1.5^o which only diagnosed the top layer elements. The fluorocarbon photoelectron intensity, at 1.5^o and 10.0^o at both surface conditions, is demonstrated by the C 1s spectra in Fig.2. Only the fluorocarbon layer intensity increased at total reflection. The C-C peak was mainly constant due to it is not originated from the layer. Since the C-C peak remains approximately constant

with angle, C and O is assigned to contamination. The angular deviation of the beam was ($\pm 0.5^{o}$). The intensity of C 1s peak at 293.3 eV increased in the region of total reflection. The total reflection condition mainly exhibited the top layer peaks at both wide and narrow scans. Beside the less fluorine after cleaning, no substantial difference was found after burnishing. Measurement at total reflection mainly exhibited the top layer elements. The TRXPS measurement produced the same data when we used a different hard disk.

This chapter reports the reproducibility of a TRXPS measurement of a hard disk storage media top layer in different conditions and demonstrates it applicability to routine application in chemical analysis.

5.4 Conclusion:

In summary, we have carried out TRXPS measurements on a typical hard disk storage media and compared them to non-total reflection X-ray photoelectron XPS for burnished and non-burnished surfaces. The background due to inelastic scattering of photoelectrons is reduced to one half in case of TRXPS than in non-total XPS. For a hard disk storage media, elements within the probing depth were observable in TRXPS with more sensitivity and stronger intensity. TRXPS was demonstrated a useful tool for the hard disk top layer chemical state characterization, reliable and reproducible.

References:

1. A. Alshehabi, S. Kunimura, J. Kawai, Anal. Method. **2** (2010) 1555-1558.
2. A. Alshehabi, N. Sasaki, J. Kawai, Adv. X-Ray. Chem. Anal., Japan **43** (2012), in press.
3. J. Kawai, J. Electron Spectrosc. Relat. Phenom. **178** (2010) 268-272.
4. B. L. Henke, Phys. Rev. **A6** (1972) 94-104.
5. M. Mehta and C.S. Fadley, Phys. Lett. **55A** (1975) 59-61.
6. M. Mehta and C.S. Fadley, Chem. Phys. Lett. **46** (1977) 225-230.
7. M. J. Chester and T. Jach, Phys. Rev. **B48** (1993) 17262-17270.
8. K. Hayashi, S. Kawato, T. Horiuchi, K. Matsushige, Y. Kitajima, H. Takenaka, and J. Kawai, Appl. Phys. Lett. **68** (1996) 1921-1923.
9. J. Kawai, H. Amano, K. Hayashi, T. Horiuchi, K. Matsushige, and Y. Kitajima, Spectrochim. Acta, Part **B 52** (1997) 873-879.
10. M. J. Chester and T. Jach, J. Vac. Sci. Technol. **B 11** (1993) 1609-1613.
11. S. Mickevičius, S. Grebinskij, V. Bondarenka, H. Tvardauskas, B. Vengalis, K. Šliužienė, B.A. Orlowski and W. Drube, Opt. Appl. **36** (2006) 235- 243.
12. M. J. Chester and T. Jach, and S. M. Thurgate, Nucl. Instrum. Methods **347A** (1994) 507-509.
13. J. Kawai, S. Kawato, K. Hayashi, T. Horiuchi, K. Matsushige, and Y. Kitajima, App. Phys. Lett. **67** (1995) 3889-3891.
14. M M. J. Chester and T. Jach, and S. M. Thurgate, Rev. Sci. Instrum. **65** (1994) 339-342.

15. T. Jach, J. Gormley, and S. Thurgate, Spectrochim. Acta, Part **B 54** (1999) 1539-1544.

16. J. Kawai, M .Takami, M. Fujinami, Y. Hashiguchi, S. Hayakawa, and Y. Gohshi, Spectrochim. Acta, Part **B 47** (1992) 983-991.

17. J. Kawai, S. Hayakawa, Y. Kitajima, K. Maeda, and Y. Gohshi, J. Electron Spectrosc. Relat. Phenom. **76** (1995) 313-318 .

18. L.G. Jacobsohn, D.F. Franceschini,M.E.H. Maia da Costa, and F.L. Freire Jr., J. Vac. Sci. Technol. **18A** (2000) 2230-2238 .

19. T. E. Karis, G. W. Tyndall, D. Fenzel-Alexander, and M. S. Crowder, J. Vac. Sci. Technol. **15A** (1997) 2382- 2387.

20. C. Donnet, J. Fontaine, A. Grill, V. Patel, C. Jahnes, and M. Belin, Surf. Coat. Technol. **94** (1997) 531-536.

21. D. T. Clark, W. J. Flast, P. J. Tweedole, and H. R. Thomas, J. Polym. Sci., Polym. Chem. Ed. 1980; 1651, 18.

Figures:

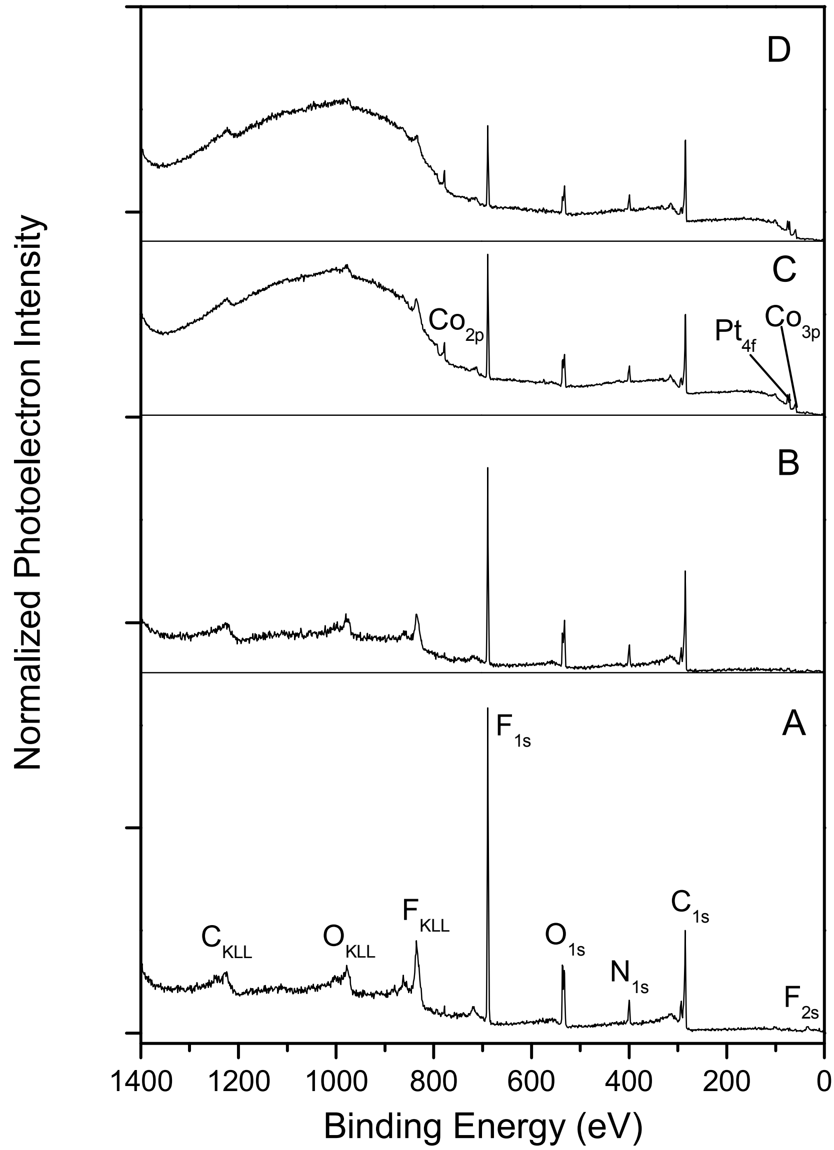

Fig 1: XPS wide scan of a typical hard disk media, A) non-treated at total reflection (1.5^o), B) Acetone-cleaned at total reflection (1.5^o), C) non-treated at non-total reflection (10°) and D) Acetone-cleaned at non-total reflection (10°) conditions. Normalized to C 1s.

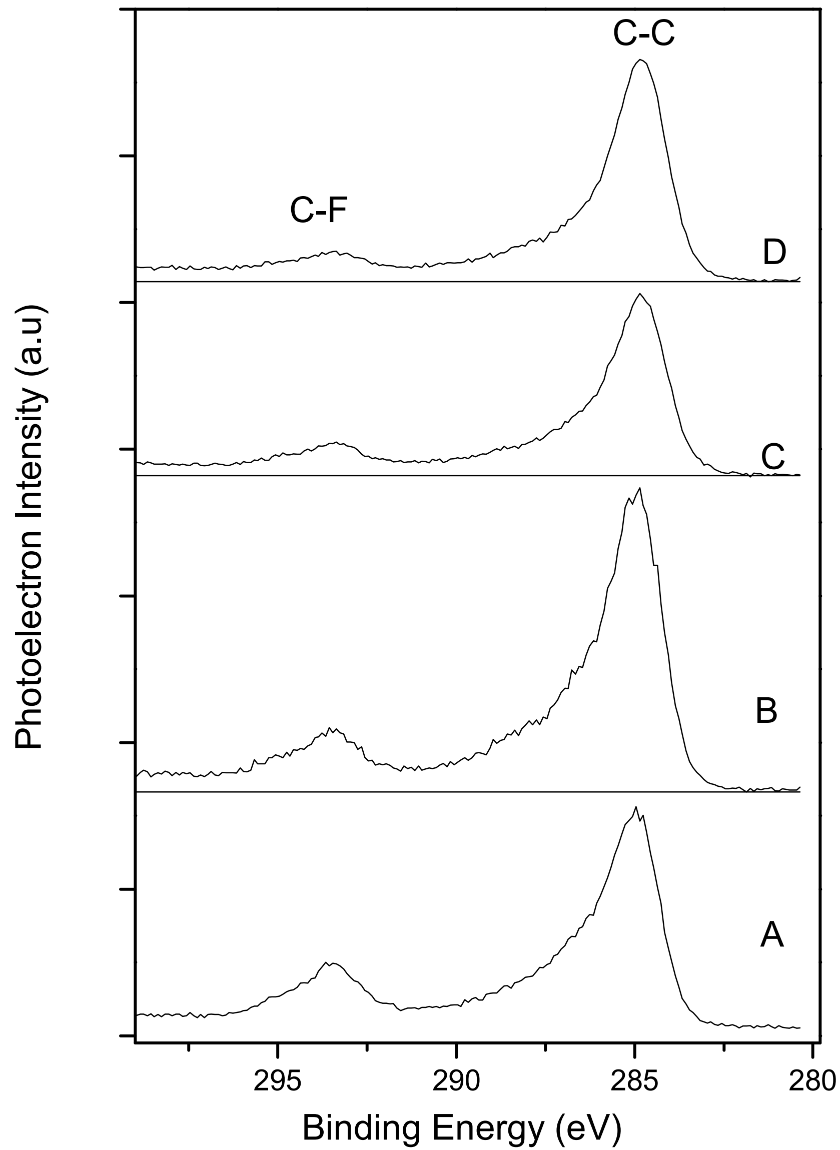

Fig 2: C 1s narrow scan of a typical hard disk media at C 1s (293.3 eV binding energy); A) non-treated at total reflection (1.5^o), B) Acetone-cleaned at total reflection (1.5^o), C) non-treated at non-total reflection (10°) and D) Acetone-cleaned at non-total reflection (10°) conditions.

Chapter 6: Extrinsic and intrinsic contributions to XPS plasmon peaks

Abstract:

Quantum interference between intrinsic and extrinsic satellites in X-ray photoelectron Spectroscopy (XPS) as well as in Auger Electron Spectra (AES), is falsified for plasmon loss peaks higher than the first order. The line width of meaured reflected electron energy loss spectra was measured and analyzed by substracting the shirley background. The extrinsic and intrinsic contributions were experimentally distinguishable for the plasmon peaks by the line width comparison. The first-order plasmon peak may also be interpreted by the method.

Plasmons in X-ray photoemission Spectroscopy (XPS) may be excited either in an extrinsic process by the photoelectron on its way out of the metal or in an intrinsic process by the core hole potential created at the moment of the X-ray absorption [1,2]. It is believed that both the extrinsic and intrinsic processes are the same for initial and final states and thus interfere with each other quantum-mechanically. Unless an observed spectrum is projected onto the extrinsic and intrinsic components, discrimination between both the extrinsic and intrinsic components is impossible by the interference picture [3,4].

Although interfernce holds correct for the first plasmon peak, it does not fully explain higher-oder plasmon peaks [5]. With the different line–shapes of higher-order plasmons, the interefence picture is not valid. The photoelectron energy shifts to a first plasmon peak if the photoelectron loses its kinteic energy, absorbed by a plasmon, in the extrinsic process. Since the life time of a plasmon is shorter, it makes a broader photoelectron peak. Higher order plasmons also get broader when a sequential plasmon is created due to photoelectron travelling in

the solid. For the intrinsic case, high-order plasmons are created when the core hole is created. Higher-order plasmons have negligibly shorter lifetimes due to their highly excited states and results in the same line width, in the first order approximation, for them all. The contribution of each, extrinsic and extrinsic, is consequently known by extrapolating the intensity of intrinsic or extrinsic plasmons of higher order down to the first order for the first order plasmon. We conclude that the intrinsic and extrinsic processes do not interfere and the contribution of each can be calculated. Fujikawa [6, 7] describes the extrinsic and intrinsic processes based on the interference picture in all plasmon peaks. Although he only described the first order plasmon, his papers' conclusion was that the interference concept holds for higher order plasmons.

In this chapter we show that the interference picture is only valid for the first peak. The method shown in this chapter may also explain the plasmon first peak.

In the extrinsic case, the electron energy spectra have energy loss progressions of plasmons, i.e. the incident electron collides several times in the solid losing the energy in discrete amounts in each collission, this energy is then absorbed by plasmons. In the intrinsic case, the impact of the first incident electron creates a longitudnal wave of higher-order plasmons instantaneously [8, 9] .The first-order plasmon is the same for both cases. Above definitions of extrinsic and intrinsic processes, based on the energy loss spectra (EELS), yield to the same relation of the line width in both photoelectron and EELS plasmons. EELS plasmons may consequently be analyzed through the line width brodening as the plasmon goes to higher orders.

Goto *et al.* measured reflected electron energy loss spectra of varoius incident electron beam energies [10-12]. We have analyzed Goto's spectra by substracting the shirley background, as shown in Fig.1. Plasmon peak seperation (15 eV) is negligibly small difference at 2 keV and the spectrometer resolution in Goto's experiment may be, with good extent, regarded constant. The higher order plasmons are observable in almost all Goto's spectra, indicating that the broadenings are smaller than those expected in the extrinsic case. Fig.1, 2 and 3 show a) the shirley background of the Shirley background for Goto's measurement of incident electron beam (2 keV) on a Si target. And b) the line-widths of the peaks are almost the same, getting a little broader in high-order plasmon peaks for the same spectrum. Fig.4 shows the difference between the exponential function $e^{-(\frac{E}{KT})}$ and experimental data. The best fit is around 1:0.84 contribution ratio of both extrinsic and intrinsic. The plasmon temperature at equilibrium was in the order of 10^6 K.

In conclusion; and opposite to the common understanding, the interference picture of the intrinsic and extrinsic contributions to plasmon satellites was falsified for plasmon satellites higher than the first-order plasmon peak. The suggested method not only provides how much each the intrinsic and extrinsic processes contribute to the plasmon peaks in the higher-orders but also may be applied to the first-order pasmon peak. Like photoelectron plasmons, electron plasmon energy loss may be classified to extrinsic and intrinsic. The extrinsic process in EELS is similar to XPS but the intrinsic is a little different between both. The first perturbation in XPS and Auger Electron Spectra (AES) is due to a core hole

creation where it is due to electron impact in EELS. For high energy limits ,e.g. 2 keV incident electron beam, however, the XPS, AES and EELS show the same intrinsic behavior. Previous studies [13] along with the AES are supporting the present conclusion. Intrinsic and extrinsic intensity is best analysed by the sum rule since the response to a test charge is leading to a sum rule [14].

References

1. J. Kondo, *The Physics of Dilute Magnetic Alloys* (Shokabo, Tokyo, 1983), p.113.
2. S. Doniach, E. H. Sondheimer, *Green's Functions for Solid State Physicists* (Imperial College Press, London, 1998), Chapter 9.
3. T. Uwatoko, H. Tanaka, K. Nakayama, S. Nagamatsu, K. Hatada, T. Konishi, T. Fujikawa, T. Kinoshita, A. Harasawa, A. Kakizaki, J. Surf. Sci. Soc. Japan, **22** (2001) 497-503.
4. S. Takayama, J. Kawai, Adv. X-Ray Chem. Anal. Japan. **39** (2008) 161-178.
5. J. Kawai, S. Takayama, L. Kövér, Journal of Surface Analysis. (to be published).
6. T. Fujikawa, Z. Phys. B-Cond. Matter. **54** (1984) 215-223.
7. T. Fujikawa, J. Phys. Soc. Japan. **55** (1986) 3244-3275.
8. C. J. Powell, J. B. Swan, Phys. Rev. **115** (1959) 869-875.
9. D. Pines, P. Nozières, *The Theory of Quantum Liquids* (Perseus, Camridge, MA (1966, 1990, 1999)), Vol. 1, Chapter 4.
10. Y. Takeichi, K. Goto, Surf. Interface Anal. **25** (1997) 17-24.
11. W. Y. Li, A. A. Iburahim, K. Goto, R. Shimizu, J. Surf. Anal. **12** (2005) 109-112.
12. COMPRO, Absolute AES spectral database, http://www.sasj.gr.jp /COMPRO.
13. F. Bechstedt, Phys. Stat.Sol. **b112** (1982) 9-49.
14. J. Kawai, in *Hartree-Fock-Slater Method for Materials Science, The DV-Xα Method for Design and Characterization of Materials*, (Springer-Verlag, Berlin, Heidelberg, 2006) Eds. H. Adachi, T. Mukoyama, J. Kawai, Chapter 9.

Figures:

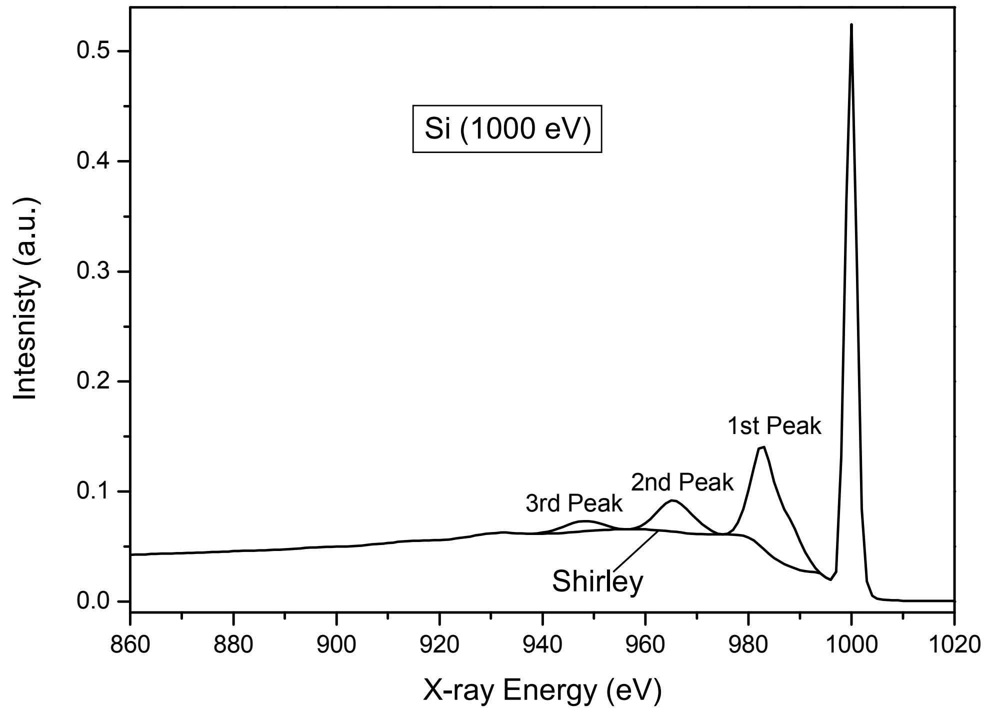

Fig 1: a) Shirley background for Goto's measurement of incident electron beam (1 keV) on a Si target.

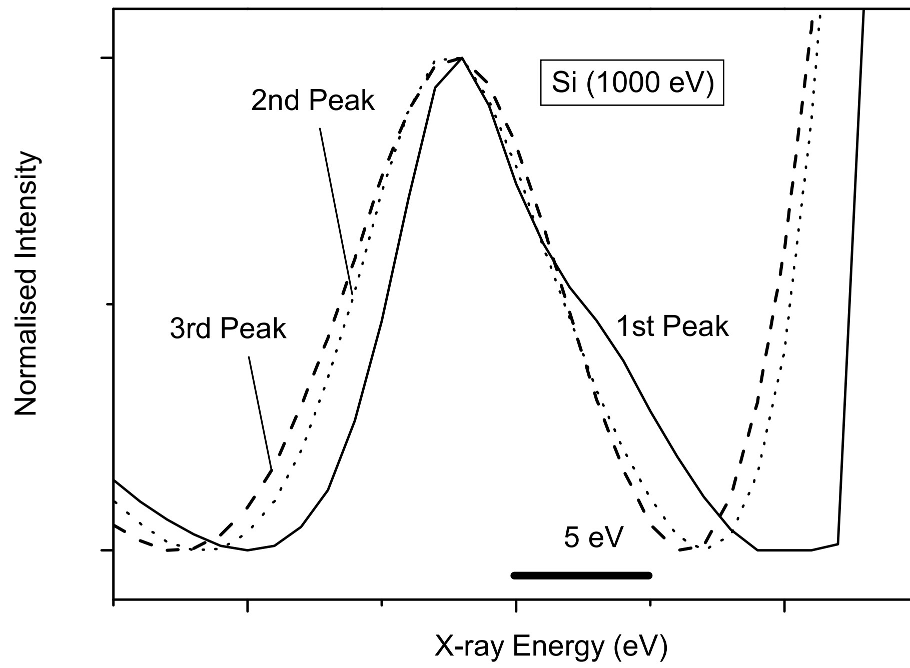

Fig 1: b) Plot of 1st , 2nd, and 3rd plasmon peaks after subtraction of background, for Goto's measurement of incident electron beam (1 keV) on a Si target.

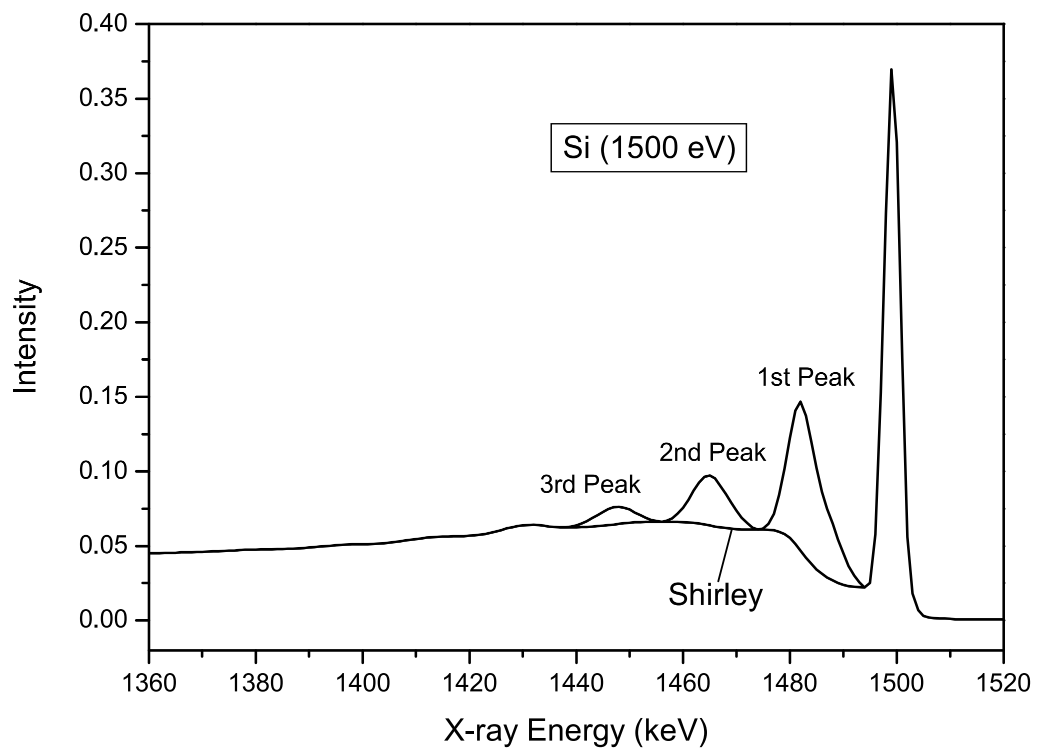

Fig 2: a) Shirley background for Goto's measurement of incident electron beam (1.5 keV) on a Si target.

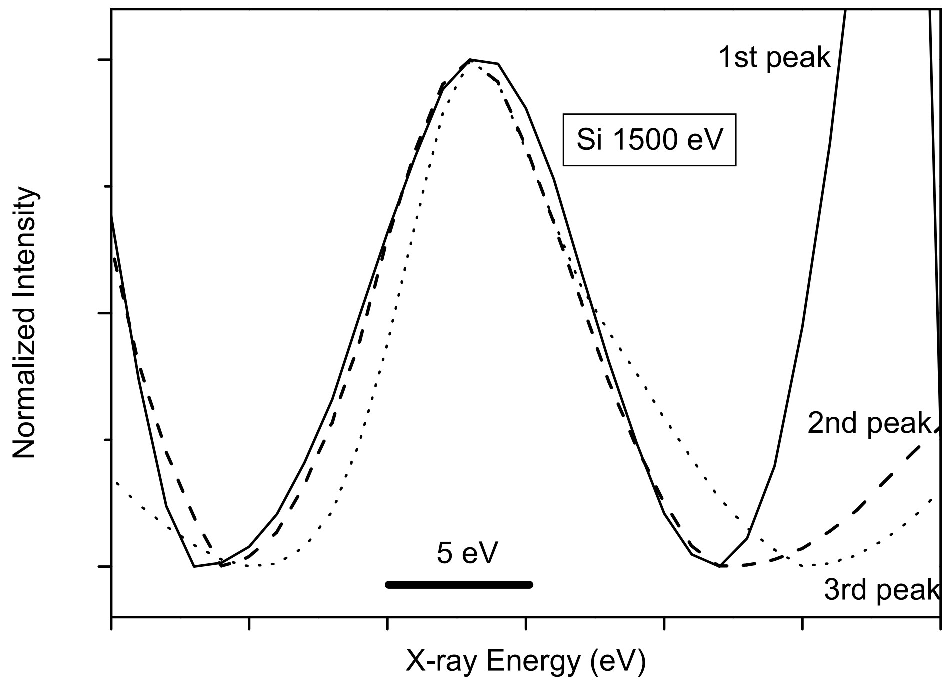

Fig 2: b) Plot of 1st , 2nd, and 3rd plasmon peaks after subtraction of background, for Goto's measurement of incident electron beam (1.5 keV) on a Si target.

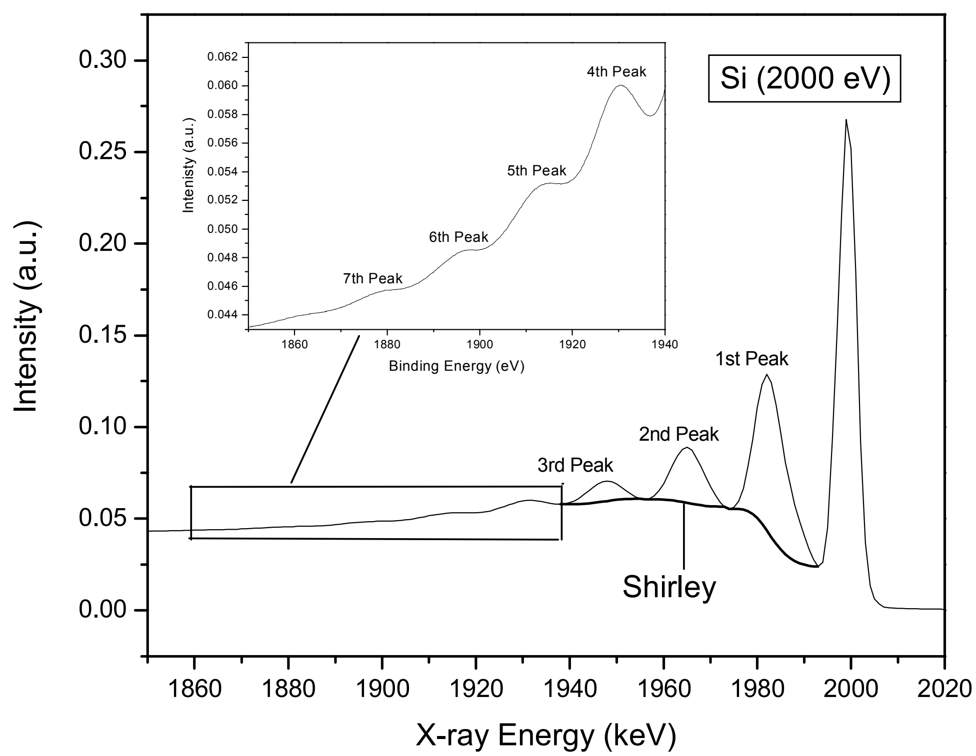

Fig 3: a) Shirley background for Goto's measurement of incident electron beam (2 keV) on a Si target.

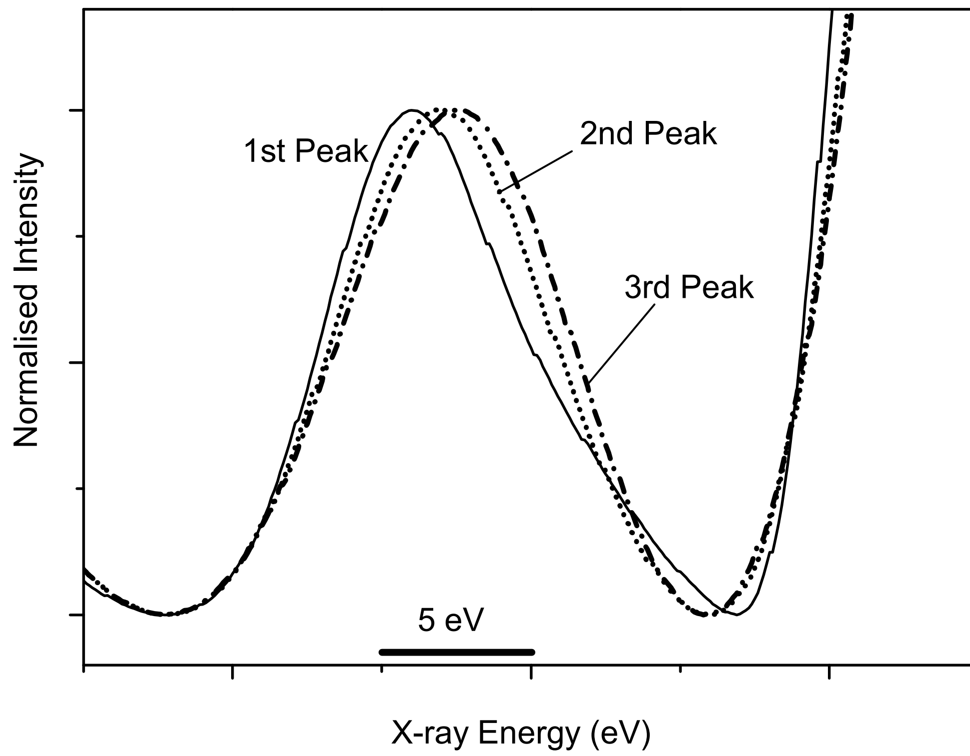

Fig 3: b) Plot of 1st , 2nd, and 3rd plasmon peaks after subtraction of background, for Goto's measurement of incident electron beam (2 keV) on a Si target.

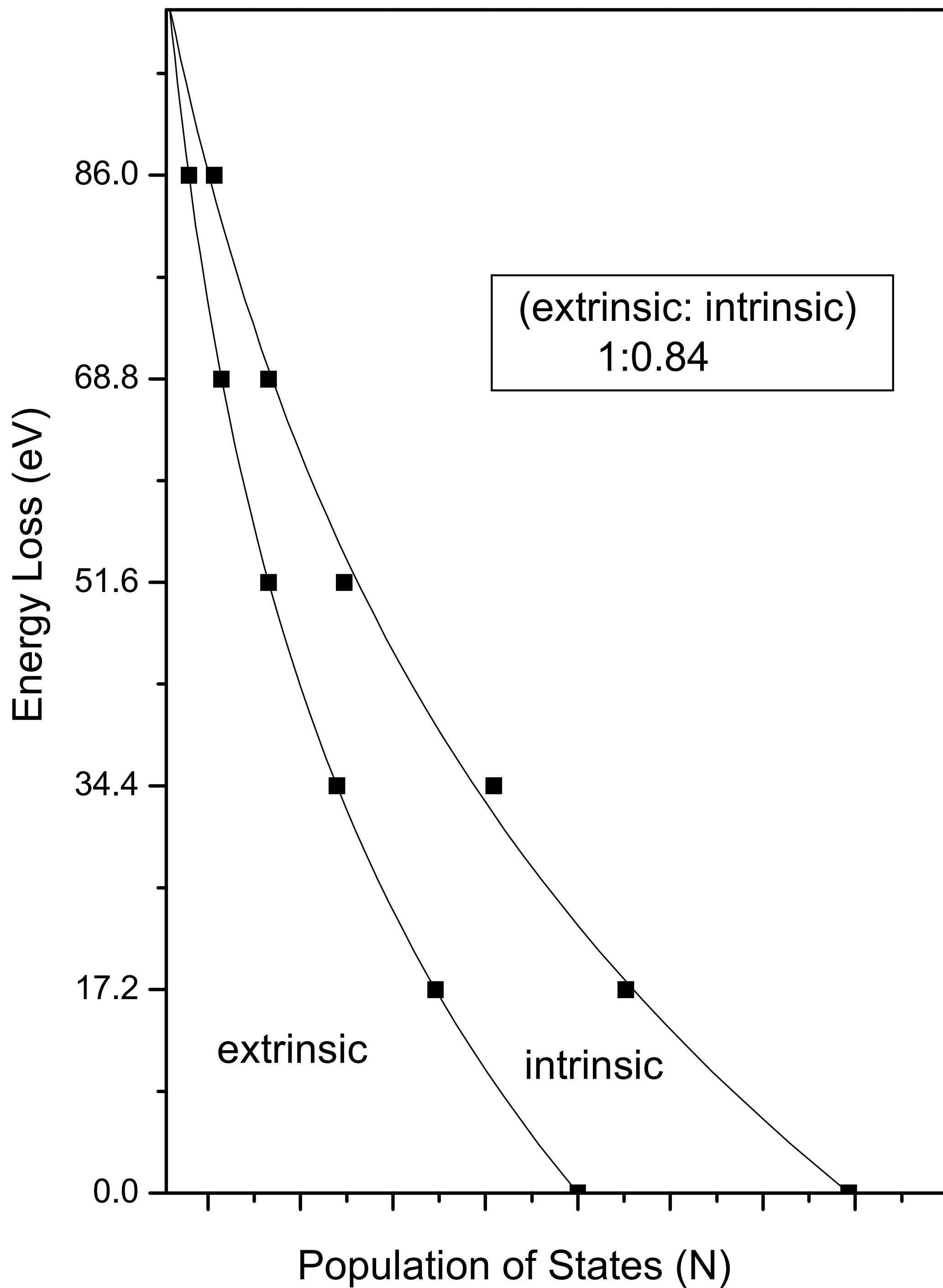

Fig 4: Comparison of extrinsic and intrinsic contributions for 2 keV electron beam into Si. It shows a 1:0.84 mixture of extrinsic : intrinsic contribution ratio.

Chapter 7: X-ray photoelectron-induced surface plasmon spectroscopy

Abstract:

We have studied the θ dependence of the plasmon excitations in the Si 2s using X-ray photoelectron emission spectroscopy (XPS) both at grazing photoelectron emission spectroscopy (TRXPS) and non- grazing emission angles. Beside the enhanced intensity at grazing emission, the ratio between the bulk and surface plasmons remains constant at a specific angle.

7.1 Introduction:

Although the origin of plasmon excitations in photoelectron emission spectroscopy (XPS) has been under investigation for decades, the relation between surface and bulk plasmon excitations has not been thoroughly investigated. Bulk plasmons are longitudinal oscillation modes of the electron gas in the solid, and are given by the condition $\varepsilon = 0$, where ε is the bulk dielectric function. The surface plasmon is an oscillating sheet of charge located at the surface, although its energy is dictated by the bulk property ($\varepsilon = -1$). Plasmon excitations may occur due to discrete energy losses associated with the movement of the photoelectrons from the excitation site through the solid to the surface; these are termed “extrinsic”. Or during the ionization event itself; these are termed “intrinsic”. Although many theoretical studies have been performed to evaluate the contributions of the intrinsic and extrinsic processes and their origin in photoelectron emission spectroscopy, the contribution of each is not yet quantified experimentally [1, 2]. Since the contributions of each are expected to

change as functions of the emission angle θ; we have studied the θ dependence of the plasmon excitations in the Si 2s using X-ray photoelectron emission spectroscopy (XPS) both at total reflection photoelectron emission spectroscopy (TRXPS) and grazing emission. The relation between the bulk and plasmon excitation intensities has been described experimentally. The contributions of each the intrinsic and extrinsic contributions have been described as functions of the emission angle θ.

7.2 Experiment:

XPS measurements were performed with a commercially available ((JEOL XPS Spectrometer JPS 9010 TRX) using a non monochromatic Mg-$K\alpha$ (hν= 1253.6 eV) radiation on a Si wafer sample. The X-ray beam was restricted to 5 mm$\times$10 mm. The pass energy was 50 eV for the wide scan measurement, 5 eV for the narrow scan and the base pressure of the vacuum chamber was (10^{-6} Pa). The spectra were obtained with an electron spectrometer consisting of a concentric hemispherical micro-channel plate type analyzer with a 10 cm long central orbital radius. The spectrometer was calibrated by reference to the Au 4f photoelectron peak. The X-ray tube input was 10 kV and 20 mA and the intensity counting rate of the spectrometer was 13500 cps with 5 channels per second. The dwell time was 200 ms/channel. The spectra were integrated for 1-2 times in wide scans and for 4-30 times in narrow scans for a better data resolution. Due to geometric restrictions in the XPS spectrometer; the angle between the detector and the non monochromatic X-ray tube is fixed to 56°, the angle was changed by tilting the

sample. The sample was tilted manually. Measurements were carried out at 10°, 15°, 30° and 62° to the surface at both incidence and emission angles. The Si wafer sample was cleaned by 500 V Argon ion sputtering prior to the (XPS) investigation. No electron charging was observed during measurement. Due to geometrical restrictions, the X-ray tube lowest incidence and emission angle is 10°. Fig. 1 shows a schematic view of the experimental setup.

7.3 Results and discussions:

Si 2s spectra, by a non monochromatic Mg-$K\alpha$ (hν= 1253.6 eV) radiation on a Si wafer sample, recorded at grazing incidence (114°) , nearly normal (62°) and grazing (10°) emissions, are shown in Fig. 2. An enhancement in the intensity of the surface plasmon (1ω_s) in the grazing emission is found at 158.5 eV binding energy (BE). Besides the intensity enhancement, there is a drastic change in the line shape between (62°) and grazing emissions in Fig. 2. In (62°) emission angle, the surface plasmon has an unusual shape with a gradually decreasing intensity towards the higher loss energy (or BE) side. In contrast to the surface plasmon, the bulk plasmon (1ω_p) intensity decreases in the grazing emission compared to (62°) emission angle. The ratio between the surface and bulk plasmon excitation intensities remains approximately constant after the emission angle (62°). The ratio between the surface and bulk plasmon excitation intensities as a function of the emission angle of Si 2s spectra by a non monochromatic Mg-$K\alpha$ (hν= 1253.6 eV) radiation on a Si wafer sample is shown in Fig.3. This is attributed by the authors to the intrinsic contribution of the bulk plasmon that is angle independent.

The extrinsic contribution is then distributed at the surface and bulk plasmon and vanishes to be a contribution of the bulk plasmon at a specific grazing emission angle.

7.4 Conclusion:

The surface plasmon excitation intensity in the spectra of Si 2s is found to increase with grazing emission. This is probably due to the large enhancement of extrinsic plasmon intensity since the intrinsic excitation is angle independent. The ratio between the surface and bulk plasmon excitation is found to be approximately constant after (62°) emission angle. This is probably due to the extrinsic excitation is the main contribution to the surface plasmon intensity and the intrinsic excitation is the main contribution in the bulk plasmon intensity after (62°) emission angle. Attributed to the above observations, the surface plasmon excitation is merely extrinsic and the separation between the intrinsic and extrinsic contributions can be done experimentally. These observations may also lay the foundation for a theory of the surface plasmon line shape as a function of the emission angle θ, which does not exit in the literature.

References:

1. S. Takayama, J. Kawai, Adv. X-Ray Chem. Anal. Japan, **39** (2008) 161-178.
2. P. Steiner, H. Höechst, and S. Hüfner, Z. Phys. B: Condens. Matter, **30** (1978)129- 143.

Figures

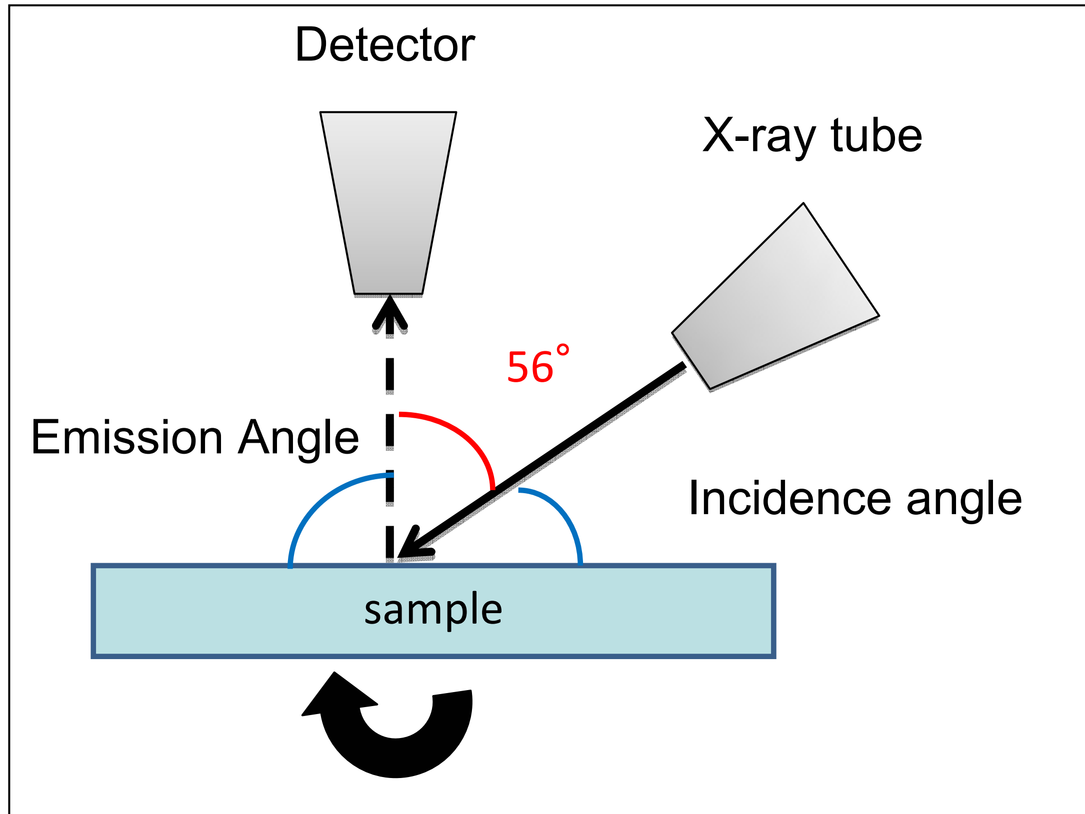

Fig. 1: a schematic view of the experimental setup.

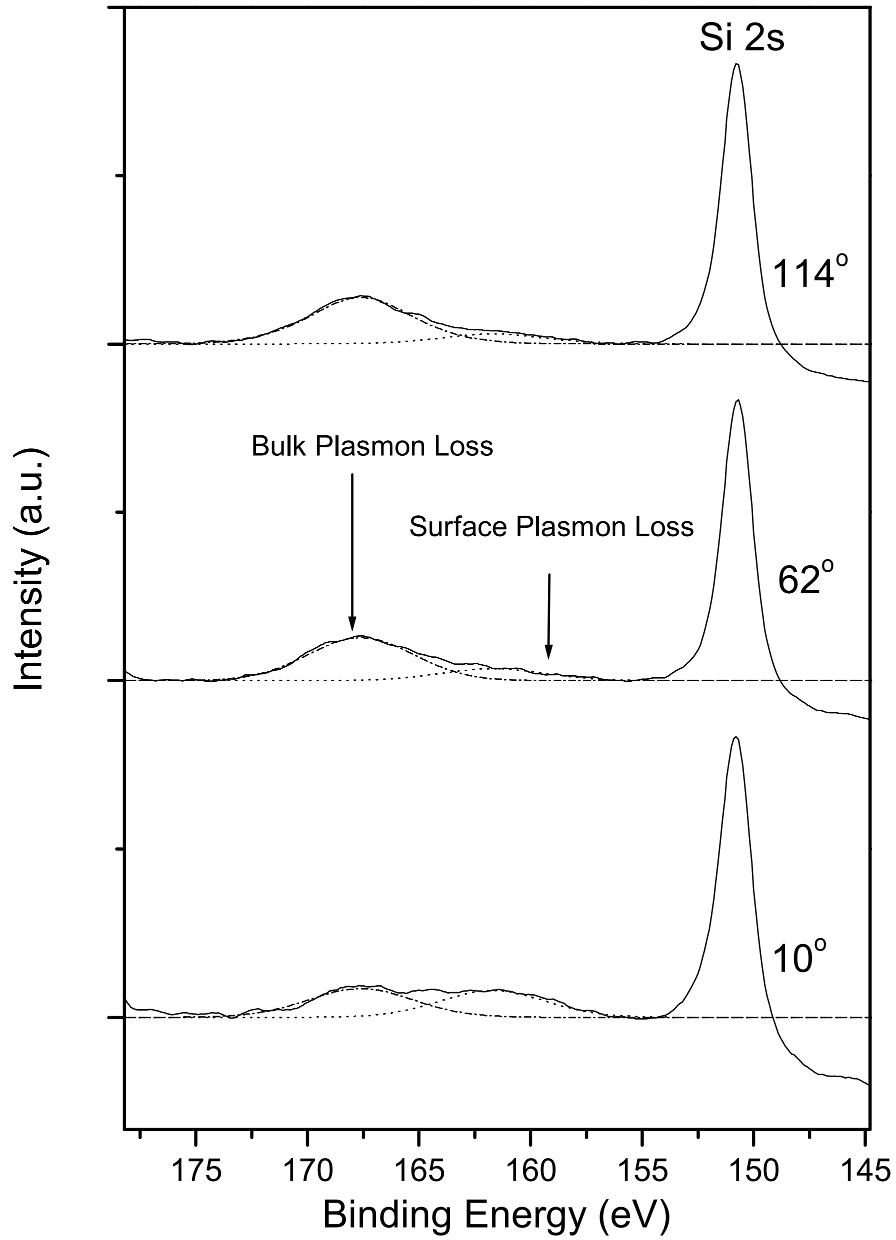

Fig 2: Si 2s surface plasmon at different emission angles. The dotted line stands for the convoluted surface plasmon , the dot-dashed for bulk and the solid for the overall spectrum.

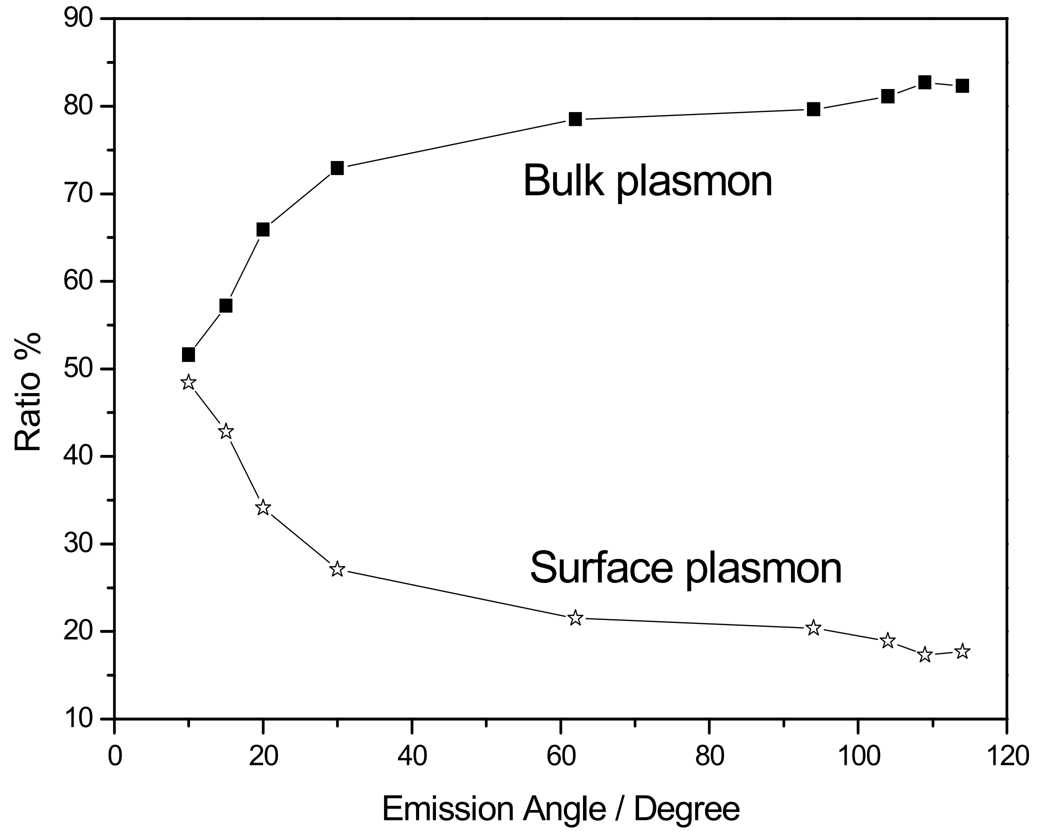

Fig. 3: The ratios of the Si 2s bulk and surface plasmon intensities at different emission angles. The surface plasmon intensity is enhanced with grazing emission.

Chapter 8: Conclusions

Based on grazing exit and grazing incidence X-ray physics, new applications of grazing X-ray analysis techniques have been demonstrated in this thesis.

In Chapter 2 we have measured X-ray intensity emitted at grazing and non-grazing angles of a Cu 45° inclined-surface. Time-consuming detector alignment to grazing exit positions in the conventional method is not needed in the 45° inclined surface method. In this method, it is possible to measure grazing exit SEM-EDX analysis without using the angle scan mechanism.

In Chapter 3 continuum X-rays are used for X-ray reflectivity measurement with a weak (1.5 watts) X-ray source. It provides the advantages of a continuum X-ray source in X-ray reflectivity; in terms of easiness of measurement; not associated with its usual problems related to strong intensity like sample damage, filter damage and provides less polychromatic effects. It also provides a portable apparatus for X-ray reflectivity. The portable apparatus is verified applicable in X-ray reflectivity measurement (XRR).

In Chapter 4 we have carried out TRXPS measurements on a typical hard disk storage media and compared them to non-total reflection X-ray photoelectron XPS. The background due to inelastic scattering of photoelectrons is reduced to one half in case of TRXPS as compared to non-total XPS. For a hard disk storage media, elements within the probing depth were observable in TRXPS with more sensitivity and stronger intensity. At TRXPS (1.5^o), mainly the top layer elements;

F, C, O, N are observable. This is proposed to be further applied on organic thin films on robust substrates. TRXPS is demonstrated as a hard disk upper layers characterization method. In Chapter 5 we have carried out TRXPS measurements on a typical hard disk storage media and compared them to non-total reflection X-ray photoelectron XPS for burnished and non-burnished surfaces. This would result in the same chemical in both cases with less intensity at burnished surfaces.

In Chapter 6, the plasmon intrinsic and extrinsic contributions were investigated by a new proposed method. The line width of Goto's meaured reflected electron energy loss spectra was measured and analyzed by substracting the shirley background. The extrinsic and intrinsic contributions were experimentally distinguishable for the plasmon peaks by the line width comparison. The first-order plasmon peak may also be interpreted by the method.

In Chapter 7, the surface plasmon excitation intensity in the spectra of Si 2s is measured at grazing emission angles. An enhancement in the intensity of the surface plasmon ($1\omega_s$) has been found in the grazing emission. The ratio between the surface and bulk plasmon excitation has been found to be approximately constant after (62°) emission angle.